Crystallographic Evidence for a New Ensemble of Ligand-Induced Allosteric Transitions in Hemoglobin: The T-to-T_{High} Quaternary Transitions[†,‡]

Jeffrey S. Kavanaugh, Paul H. Rogers, and Arthur Arnone*

Department of Biochemistry, Roy J. and Lucille A. Carver College of Medicine, The University of Iowa, Iowa City, Iowa 52242

Received October 12, 2004; Revised Manuscript Received January 19, 2005

ABSTRACT: A detailed description of hemoglobin cooperativity requires knowledge of the dimer−dimer interactions responsible for the low ligand affinity of the quaternary-T tetramer, the "quaternary-T constraints", along with stereochemical pathways that specify how ligand binding disrupts these quaternary constraints. The recent mutagenic screen of Noble et al. [Noble, R. W., et al. (2001) *Biochemistry 40*, 12357−12368] has identified the major region of quaternary constraint to be a cluster of residues at the $\alpha1\beta2$ interface that is centered at Trp37β. In this paper, crystallographic studies are presented for most of the mutant hemoglobins studied by Noble et al. These crystallographic experiments identify structural transitions—referred to as T-to-T_{High} transitions—between the quaternary-T structure of wild-type deoxyhemoglobin and an ensemble of related T-like quaternary structures that are induced by some mutations in the Trp37β cluster and/or by exposing crystals of wild-type or mutant deoxyhemoglobins to oxygen. The T-to-T_{High} quaternary transitions consist of a rotation of the $\alpha1\beta1$ dimer relative to the $\alpha2\beta2$ dimer as well as a coupled $\alpha\beta$ dimer bending component that consists of a small rotation of the $\alpha1$ subunit relative to the $\beta1$ subunit (and a symmetry related rotation of the $\alpha2$ subunit relative to the $\beta2$ subunit). In addition, differences in subunit tertiary structure associated with the T-to-T_{High} transitions suggest two stereochemical pathways (one associated with the α subunits and one associated with the β subunits) by which ligand binding specifically disrupts quaternary constraints in the Trp37β cluster. In the α subunits, ligand binding induces a shift of the heme iron producing tension in a chain of covalent bonds that extends from the Fe−$N^{\epsilon2}$His(F8)$\alpha1$ bond to the peptide backbone bonds of residues His87(F8)$\alpha1$ and Ala88(F9)$\alpha1$. This tension induces an α-to-π transition in the COOH-terminal end of the F-helix that shifts the β-carbon of Ala88$\alpha1$ by ∼1.5 Å directly into the side chain of Tyr140$\alpha1$ (a key residue in the Trp37$\beta2$ cluster). Collectively these structural changes constitute a relatively short pathway by which ligand binding forces Tyr140$\alpha1$ into the $\alpha1\beta2$ interface disrupting quaternary constraints associated with the Trp37$\beta2$ cluster. In the β subunits, our analysis suggests a more extended energy transduction pathway in which ligand-induced $\beta1$-heme movement triggers tertiary changes in the $\beta1$ subunit that promote $\alpha1\beta1$ dimer bending that disrupts quaternary constraints in the Trp37$\beta2$ cluster at the $\alpha1\beta2$ interface.

It has long been realized that hemoglobin and all other allosteric proteins that exhibit positive cooperativity have the following general properties: (1) they are oligomeric assemblies with multiple ligand (substrate) binding sites, (2) the unliganded oligomeric protein has a ligand affinity that is much lower than that of the isolated subunits, and (3) large changes in quaternary structure and smaller changes in tertiary structure occur in response to ligand binding (*1*). Thus the initial low affinity of the oligomeric protein must be the result of subunit−subunit interactions (i.e., quaternary structure constraints) that oppose the binding of ligand. As ligand binds to the protein, its tertiary and quaternary structures change, quaternary constraints relax, and at least some of the remaining unliganded binding sites (active sites) exhibit increased ligand affinity. Positive cooperativity, therefore, is achieved by linking small ligand-induced changes in local tertiary structure to larger changes in quaternary structure.

In the case of hemoglobin, the oxygen affinity of the deoxyhemoglobin $\alpha_2\beta_2$ tetramer is nearly 400-fold lower than the oxygen affinity of free deoxy $\alpha\beta$ dimers (*2*, *3*), indicating that quaternary constraints unique to the deoxy tetramer's dimer−dimer interface oppose ligation-induced structural transitions. Identifying these quaternary constraints and determining how they are stereochemically linked to ligand binding is central to a full understanding of the cooperative mechanism of hemoglobin action. Early studies by Antonini et al. (*4*) and Kilmartin et al. (*5*, *6*) on carboxypeptidase A and carboxypeptidase B digested human hemoglobin showed that loss of the COOH-terminal residues of the α subunits (desArg141α hemoglobin), and to a lesser extent the COOH-terminal residues of the β subunits (desHis146β hemoglobin), increased the overall ligand affinity of hemoglobin (i.e., the oxygen pressure required for half saturation, the p50, decreased). Since the initial crystal structures of liganded

[†] This work was supported by National Institutes of Health Program Project Grant PO1 GM58890.

[‡] Refined coordinates and structure factors for 34 deoxyhemoglobins and 19 liganded hemoglobins have been deposited in the RCSB Protein Data Bank. PDB codes are included in Table 1.

* Correspondence should be addressed to this author. E-mail: arthur-arnone@uiowa.edu.

10.1021/bi047813a CCC: $30.25
Published on Web 03/29/2005

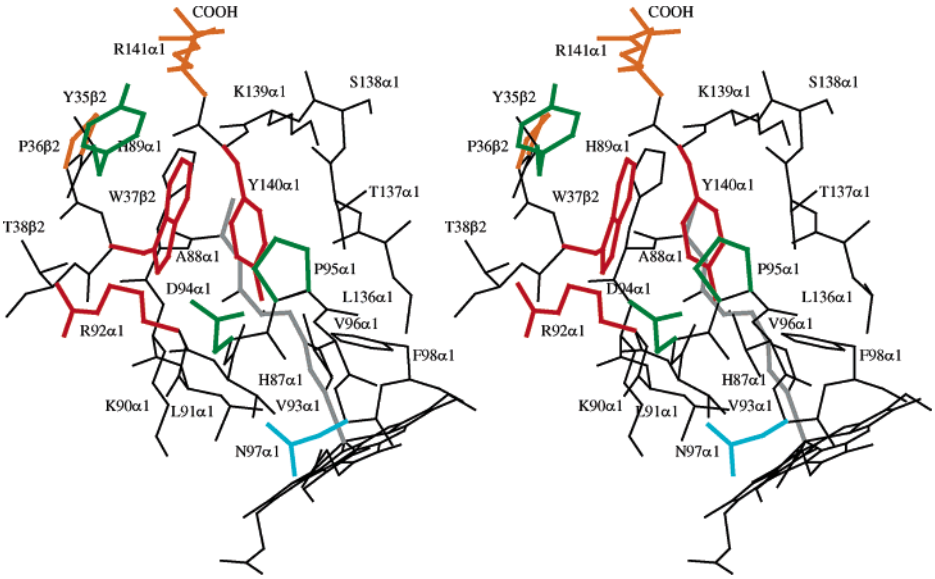

FIGURE 1: Stereoimage of the hinge region of the α1β2 interface in the wild-type quaternary-T deoxyhemoglobin tetramer. The side chains of the amino acid residues are color-coded according to the ratio of the mutant to wild-type CO-combination rate constants as reported by Noble el al. (*14*) as follows; red >5, orange 2.6−5, green 1.6−2.5, and light blue 0.7−1.5. The mutationally sensitive sites in this region (the red, orange, and green residues) represent the major source of quaternary constraint in the quaternary-T deoxyhemoglobin tetramer. Collectively, this group of residues is referred to as the "Trp37β cluster". Mutations at residue Trp37β have the largest impact on the ligand affinity of the deoxyhemoglobin tetramer. Trp37β is located at the center of the cluster and makes contacts of 3.7 Å or less with each of the other members of the cluster.

and deoxyhemoglobin revealed that both the α and β COOH-terminal residues contribute to interdimer salt bridges in deoxyhemoglobin, but not in liganded hemoglobin, Perutz proposed a stereochemical mechanism for hemoglobin allostery in which these salt bridges are the major source of quaternary constraint (*7*, *8*). Subsequently, the degree to which the COOH-terminal residues of the α and β subunits contribute to the quaternary-T constraints that reduce the ligand affinity of the deoxyhemoglobin tetramer was determined by measurements of the first Adair constant, K_1, for desArg141α hemoglobin and desHis146β hemoglobin in solution and in quaternary-T hemoglobin crystals (*9*−*12*). These studies showed that the constraints associated with the salt bridges formed by Arg141α are significant while those associated with His146β are much smaller. In addition, resonance Raman studies of Wang and Spiro (*13*) have revealed that strain in the Fe−$N^{\epsilon 2}$His(F8) bonds is decreased in desArg141α deoxyhemoglobin and less so in desHis146β deoxyhemoglobin, demonstrating a direct connection between the COOH-terminal salt bridges and the heme groups.

Since the COOH-terminal salt bridges are not the only dimer−dimer interactions that are present in the deoxyhemoglobin tetramer and absent in the fully liganded hemoglobin tetramer, other ligation-dependent dimer−dimer contacts could also serve as quaternary constraints. In an effort to determine the relative importance of all the dimer−dimer interactions, Noble et al. (*14*) carried out a mutagenic screen (mainly an alanine screen) in which the interdimer contacts associated with individual residues were systematically eliminated. In particular, Noble et al. measured the second-order CO combination rate constants for 41 hemoglobin variants with mutations at 29 different residues. [The CO combination rate constant measured in the presence of inositol hexaphosphate has been shown to be an excellent proxy for K_1, the first Adair constant (a parameter that is very difficult to determine, especially for variant hemoglobins with high ligand affinity). Specifically, the CO combination rate constant correlates very well with the oxygen affinity (p50 values) of crystalline hemoglobin constrained by lattice contacts to the quaternary-T conformation (*15*) as well as with the K_1 value measured in solution for symmetric Fe/Zn hybrid hemoglobins that have only two oxygen binding sites (*12*, *16*). Thus the CO combination rate constant is a good measure of the level of quaternary constraint present in a deoxyhemoglobin tetramer.] While the majority of dimer−dimer interface mutations had little or no impact on the CO combination rate, mutations at a small number of residues (that included Arg141α, but not His146β) had a substantial impact on the CO combination rate. Moreover, these residues (i.e., the residues that contribute in a significant way to the quaternary constraints) are not distributed uniformly over the dimer−dimer interface; they are localized almost exclusively to the so-called "hinge region" of the α1β2 interface [see Figure 1 of Noble et al. (*14*)]. More specifically, these residues form a cluster centered at Trp37β (Figure 1), the residue that is most sensitive to mutation, and for this reason we refer to this critical group of residues as the "Trp37β cluster". Consistent with this finding are the proton exchange studies of Mihailescu et al. (*17*) that showed approximately 4 kcal/(mole of tetramer) of ligation-linked structural free energy is associated with Trp37β and its environment.

A number other studies have also demonstrated that Trp37β is a major source of quaternary constraint. Specifically, previous studies showed that replacing Trp37β with Tyr, Ala, Gly, and Glu results in progressively disruptive functional changes that include increasing oxygen affinity, increasing CO-combination rates, and decreasing cooperativity (*18*, *19*). For the Gly and Glu mutations (*14*, *18*, *19*), the functional properties of the hemoglobin tetramer approach those of isolated αβ dimers. These functional changes correlate well with progressively disruptive structural changes

(as observed in crystal structures of the mutant deoxyhemoglobins) that include changes in quaternary structure, changes in subunit tertiary structure, increased mobility of the α subunit COOH-terminal dipeptide, and shortening of the α and β Fe−$N^{\epsilon 2}$His(F8) bonds (*20*). The shortening of the Fe−$N^{\epsilon 2}$His(F8) bonds correlates with resonance Raman studies that show a progressive decrease in strain at these bonds (*21*). Collectively, these findings, as well as more recent crystallographic studies on quaternary-T nitrosylhemoglobin (*22*), demonstrate a direct linkage between the quaternary constraints associated with Trp37β and the ligand affinity of the heme groups. The crystallographic studies on quaternary-T nitrosylhemoglobin showed that when crystals of wild-type deoxyhemoglobin are exposed to NO the α (but not the β) Fe−$N^{\epsilon 2}$His(F8) bond is broken. In contrast, when crystals of βW37E deoxyhemoglobin are exposed to NO both the α and β Fe−$N^{\epsilon 2}$His(F8) bonds remain intact, indicating that ligand-induced strain at the α Fe−$N^{\epsilon 2}$His(F8) bond is greatly reduced when the quaternary constraints associated with Trp37β are eliminated (*22*).

The crystallographic studies reported below provide additional independent evidence for the localization of quaternary constraints to the Trp37β cluster. These studies show that as the quaternary constraints are disrupted by mutation or by ligand binding the hemoglobin tetramer undergoes a series of progressive quaternary transitions from the quaternary-T structure of wild-type deoxyhemoglobin to an ensemble of related T-like quaternary structures. Analysis of the tertiary and quaternary changes in these structures reveals different stereochemical pathways for the α and β subunits by which ligand binding specifically disrupts quaternary constraints in the Trp37β cluster.

MATERIALS AND METHODS

Preparation and Crystallization of Variant Hemoglobins. Preparation of the variant human hemoglobins by the core facilities of NIH sponsored Program Project Grant GM-58890 was described previously (*14*). Due to differences in amino terminal processing in *Escherichia coli* and humans, the recombinant proteins also have innocuous αV1M or βV1M mutations (*23*−*26*).

Crystals of all the variant hemoglobins were grown at room temperature in the deoxy form from PEG[1] solutions as first described by Ward et al. (*27*) with the addition of a seeding step (*20*, *28*). In summary, deoxyhemoglobin crystals were grown from solutions consisting of 10 mM potassium phosphate at pH 7.0, 100 mM potassium chloride, 3 mM sodium dithionite, 10.0% PEG 6000, and 10 mg/mL hemoglobin. All solutions were deoxygenated with pure nitrogen, and all the crystallization and crystal handling procedures were carried out in a nitrogen-filled glovebox or glovebag. In order to collect diffraction data under anaerobic conditions, crystals were washed in substitute mother liquor that contained all the nonprotein components of the original crystallization solution, but with the PEG concentration increased to 13%, and then mounted under nitrogen in quartz capillaries for data collection.

Exposing Crystals of Deoxyhemoglobin to Oxygen. For some variant hemoglobins diffraction data also were collected after exposure to oxygen. In the case of the 37β mutants, the crystals were exposed to oxygen by simply opening the capillary tube to air. In contrast, crystals of wild-type deoxyhemoglobin and the non-β37 mutants disorder when exposed to air at room temperature. However, Paoli et al. (*29*) found that, at 4 °C and in the presence of IHP (inositol hexaphosphate), wild-type deoxyhemoglobin crystals can bind oxygen to all four heme groups without disordering. In the present study, a similar procedure was used to expose crystals of wild-type deoxyhemoglobin and the non-β37 mutants to oxygen. Specifically, deoxyhemoglobin crystals first were stabilized by soaking for approximately 18 h in the substitute mother liquor mentioned above with the PEG concentration increased to 20% and the addition of 2.2 mM IHP. Once soaked, the crystals were transferred anaerobically to a substitute liquor that did not contain dithionite and cooled to 4 °C. Finally, at 4 °C, the crystals were exposed to oxygen for 2 h, at a pressure of 1 atm, and then mounted in oxygen-filled quartz capillaries. Twelve hours after the crystals were exposed to oxygen, diffraction data were collected at −4 °C. Similar experiments with wild-type deoxyhemoglobin crystals also were carried out with IHP concentrations of 5 mM, 10 mM, and 20 mM in order to study the effect of IHP concentration on ligand-induced structural changes.

Diffraction Data Collection. For some crystals, diffraction data were collected with a Rigaku RU200 rotating anode generator that was fitted with an AFC6 diffractometer, a graphite monochromator, and a San Diego Multiwire Systems area detector. The diffraction data for other crystals were collected with a Rigaku RU200 rotating anode generator that was fitted with Osmic Confocal Max-Flux Optics and an R-AXIS IV^{++} area detector from Molecular Structure Corporation. All the diffraction data were collected on unfrozen crystals. For data collected with X-rays filtered by the graphite monochromator, the hemoglobin crystals were mounted in sealed quartz capillary tubes in the usual way (i.e., they were held in place by surface tension against the inner wall of the capillary tube). However, crystals mounted in this way degraded rapidly when exposed to X-rays filtered by the Osmic Confocal Max-Flux Optics. This problem was circumvented by mounting the hemoglobin crystals in sealed capillary tubes that were completely filled with the substitute mother liquor. In this case, the crystals were held in place with cotton fibers (*30*). Diffraction data collected on the San Diego Multiwire Systems area detector were scaled and merged according to the procedures of Howard et al. (*31*). Diffraction data collected on the R-AXIS IV^{++} area detector were processed using the MOSFLM (*32*) and SCALA (*33*) programs as incorporated in the CCP4 software package (*34*). Diffraction data statistics are summarized in Table 1.

Refinement of Deoxyhemoglobin Structures. The initial atomic model for each of the β subunit variants was the tetrameric deoxy βV1M structure (*26*) in which the mutated residue was replaced with alanine (or by glycine in the case of the glycine mutations). The initial atomic model for each of the α subunit variants was the tetrameric structure of wild-type deoxyhemoglobin (*35*) in which the mutated residue was replaced with alanine (or glycine where appropriate). (Met1α was modeled as an alanine residue throughout the refinement process because the methionine side chain atoms are disordered and not visible in electron density images.) These starting models were subjected to rigid-body refine-

[1] Abbreviations: PEG, polyethylene glycol; rms, root-mean-square.

ment using X-PLOR (*36*) as described previously (*22*) followed by either least-squares refinement with PROLSQ (*37*) or maximum-likelihood refinement using REFMAC5 (*34*, *38*). Structural changes outside the radius of convergence of PROLSQ or REFMAC5 were manually incorporated with the TOM/FRODO software (*39*, *40*). In all cases, the diffraction data were split into test and working data sets that comprised 10% and 90% of the total X-ray diffraction data, respectively. The test and working data sets for the α subunit and β subunit variants were matched to those of wild-type deoxyhemoglobin and deoxy βV1M, respectively, to allow for the calculation of the R_{free} statistic (*41*) throughout the refinement process. Refinement statistics are summarized in Table 1.

Refinement and $R_{free}^{local-5}$ Cross-Validation of Oxygenated Hemoglobin Crystal Structures. Each oxygenated crystal structure was refined and the oxygen-induced structural changes validated using the protocols recently described by Chan et al. (*22*). In brief, each deoxyhemoglobin diffraction data set was randomly divided into a test data set consisting of 10% of the data and a working data set consisting of the remaining 90% of the data. The deoxyhemoglobin atomic model was debiased (*42*) relative to the test data set by carrying out more than 600 cycles of maximum-likelihood refinement using REFMAC5. The resulting model was used as a starting model for refinement against the corresponding oxygenated diffraction data that were divided into the same test and working data sets as the deoxy diffraction data. The refinement consisted of rigid-body refinement using X-PLOR followed by maximum-likelihood refinement using REFMAC5. (Only rigid-body refinement was run for the IHP stabilized βY35A crystal exposed to oxygen because the diffraction data for this crystal are very low resolution (Table 1).) Structural changes outside the radius of convergence of REFMAC5 were manually incorporated with the TOM/FRODO software. During the process, oxygen ligands were added to the atomic model, but a molecule of IHP was not included. [As stated above, IHP was added to crystals of wild-type deoxyhemoglobin and crystals of the non-37β deoxyhemoglobin variants in order to prevent crystal disordering after exposure to oxygen. However, a molecule of IHP was not added to these atomic models because little or no significant electron density was observed for IHP in its binding site at the entrance to the central cavity between the β subunits. Waller and Liddington, working with the same crystal form of the deoxyhemoglobin−IHP complex, also reported very weak electron density for IHP (*43*). Since the addition of IHP prevents oxygen-induced crystal disordering (*43*), IHP apparently binds to and stabilizes the quaternary-T hemoglobin tetramer. However, in this orthorhombic crystal lattice it must bind in a more disordered mode than in the monoclinic crystal lattice previously used by Arnone and Perutz to study the deoxyhemoglobin−IHP complex (*44*).]

The $R_{free}^{local-5}$ statistic (*20*, *22*) was used to validate tertiary structure changes induced by oxygenation of the deoxyhemoglobin crystals. This statistic uses the unbiased test data set to cross-validate small tertiary structure differences between the deoxy and oxygenated crystal structures. That is, the localized oxygen-induced changes in tertiary structure that were introduced during the second stage of the refinement (the REFMAC5 and TOM/FRODO refinement) were cross-validated through the use of "hybrid" atomic models. Specifically, after convergence of the final REFMAC5 refinement cycles, hybrid atomic models were generated by replacing the coordinates of each pentapeptide in the final REFMAC5 refined model with the coordinates of the corresponding pentapeptide of the atomic model that had undergone only rigid-body refinement (but not individual atom refinement). The coordinates for each of these hybrid models were identical to those of the final refined model except for a single (unrefined) pentapeptide. The standard R_{free} value (*41*) calculated with a particular hybrid model minus the standard R_{free} value calculated with the final atomic model is defined as the $R_{free}^{local-5}$ value associated with the replaced pentapeptide. If the structural changes associated with a particular pentapeptide represent a genuine improvement to the starting model, the corresponding $R_{free}^{local-5}$ value should be significantly greater than zero. Plotting the $R_{free}^{local-5}$ parameter versus residue number generates a profile that can be used to discriminate between small genuine structural changes and those changes in the atomic model that are due to experimental uncertainty (i.e., uncertainty associated with poorly defined regions of the electron density map).

Because only 10% of the diffraction data are used to generate a $R_{free}^{local-5}$ profile, spurious signals may appear and genuine changes in structure may not cross-validate. However, the sensitivity of the $R_{free}^{local-5}$ parameter is dramatically improved by carrying out multiple calculations with different, mutually exclusive, test data sets. That is, the $R_{free}^{local-5}$ calculation can be repeated 10 times. In each case, the calculation is started with a deoxyhemoglobin model that is debiased relative to one of 10 mutually exclusive test data sets. Averaging the 10 resulting $R_{free}^{local-5}$ profiles generates a $\langle R_{free}^{local-5} \rangle$ profile that uses of all the diffraction data to cross-validate tertiary structural changes.

Structural Analysis. The following criteria were used to identify strong noncovalent interactions at the dimer−dimer interface. For each type of interaction, a contact is counted only if each of the interacting atoms has a temperature factor of 50 Å^2 or less. A polar contact was defined as an atomic interaction of less than 3.2 Å between a pair of polar atoms. A nonpolar contact was defined as an atomic interaction of less than 3.5 Å between two nonpolar atoms or between a polar and a nonpolar atom. Interactions of 3.2−3.5 Å between two polar atoms were counted as nonpolar contacts. A water bridge was defined as a [polar atom···water···polar atom] interaction where both water hydrogen bonds are less than 3.2 Å. All interactions between 3.5 and 3.8 Å were classified as general weak contacts.

Rigid-body screw-rotation analysis (*45*, *46*) was used to characterize mutation- and ligation-induced quaternary structure transitions. These transitions have two components: an interdimer rigid-body rotation of the α1β1 dimer relative to the α2β2 dimer as well as an intradimer rigid-body rotation of an α subunit relative to a β subunit. The approach for analyzing interdimer rotation has been described in detail by Mueser et al. (*47*). In brief, the following steps are involved. First each tetramer is placed in a standard orientation with the dyad axis of the tetramer positioned along the *y*-axis of the coordinate system. Next the atomic coordinates for the backbone atoms of the α1β1 and α2β2 dimers of

Table 1: Data Collection and Refinement Statistics[a]

hemoglobin[b]	PDB code	*a* (Å)	*b* (Å)	*c* (Å)	resolution (Å)	total measurements	unique reflns	completeness (%)	av $I/\sigma(I)$	av multiplicity	R_{merge} (%)	R_{cryst}[c]	R_{free}[c]	rms bond lengths (Å)	rms bond angles (deg)	av *B* factor (Å^2)
HbA	1RQ3	97.0	99.3	66.0	1.91 (2.05−1.91)	185171 (21386)	47999 (7770)	95.3 (78.1)	13.7 (3.0)	6.7 (2.8)	4.4 (14.9)	0.165 (0.212)	0.198 (0.249)	0.018	1.84	24.8
αK40G	1XY0	97.2	99.5	66.0	1.99 (2.14−1.99)	266999 (22911)	43249 (7398)	96.8 (84.1)	7.3 (1.4)	6.2 (3.1)	8.8 (28.1)	0.189 (0.274)	0.260 (0.323)	0.012	1.30	24.9
αY42A	1XYE	97.0	99.3	66.2	2.13 (2.29−2.13)	243449 (19998)	36379 (6440)	97.9 (90.2)	5.4 (1.3)	6.7 (3.1)	5.9 (18.5)	0.192 (0.279)	0.241 (0.328)	0.021	1.97	19.7
αL91A	1XZ5	97.1	99.0	65.9	2.11 (2.27−2.11)	252035 (21223)	36432 (6491)	97.6 (88.2)	7.4 (1.7)	6.9 (3.3)	9.0 (25.2)	0.176 (0.245)	0.248 (0.298)	0.009	1.20	24.5
αR92A	1XZ7	97.1	99.1	66.1	1.90 (2.05−1.90)	127949 (19693)	45795 (7928)	90.1 (76.9)	14.5 (4.9)	2.8 (2.5)	4.5 (13.7)	0.173 (0.203)	0.203 (0.259)	0.015	1.57	27.8
αD94G	1XZU	97.0	99.7	65.7	2.16 (2.32−2.16)	239576 (20016)	34071 (6034)	97.3 (87.6)	6.9 (1.5)	7.0 (3.3)	10.8 (26.3)	0.179 (0.251)	0.260 (0.319)	0.012	1.50	24.7
αP95A	1XZV	97.2	99.1	66.0	2.11 (2.28−2.11)	234028 (19291)	36004 (6347)	97.0 (86.7)	7.4 (1.9)	6.5 (3.0)	11.4 (22.7)	0.170 (0.220)	0.246 (0.283)	0.011	1.40	24.5
αN97A	1Y09	97.3	99.4	65.9	2.25 (2.43−2.25)	72395 (7527)	26928 (4527)	87.6 (72.5)	8.2 (4.7)	2.7 (1.7)	5.8 (14.6)	0.155 (0.189)	0.206 (0.287)	0.022	1.96	32.6
αY140A	1Y0A	96.8	99.2	65.8	2.22 (2.39−2.22)	231415 (19027)	31333 (5675)	97.9 (90.0)	7.3 (1.8)	7.4 (3.4)	9.8 (25.3)	0.175 (0.205)	0.237 (0.255)	0.011	1.50	24.6
αY140F	1Y0C	97.1	99.5	66.0	2.27 (2.44−2.27)	240421 (19438)	29663 (5366)	97.9 (89.8)	7.4 (1.9)	8.1 (3.6)	9.4 (15.0)	0.169 (0.229)	0.256 (0.317)	0.011	1.40	24.7
desArg141α	1Y0D	96.9	99.0	65.9	2.10 (2.27−2.10)	253314 (22208)	36277 (6366)	97.2 (86.5)	12.2 (2.2)	7.0 (3.5)	5.9 (18.9)	0.183 (0.238)	0.247 (0.283)	0.012	1.30	24.7
βV1M	1Y0W	97.2	99.3	65.9	2.14 (2.30−2.14)	267646 (22844)	35230 (6448)	98.1 (91.0)	11.2 (2.9)	7.6 (3.5)	7.9 (17.3)	0.166 (0.208)	0.192 (0.254)	0.014	1.68	24.8
βV33A	1Y22	97.3	99.1	66.0	2.16 (2.32−2.16)	230760 (19279)	33899 (5986)	97.4 (87.6)	10.3 (2.3)	6.8 (3.2)	8.0 (21.8)	0.178 (0.243)	0.248 (0.290)	0.010	1.30	24.8
βV34G	1Y2Z	97.1	99.3	66.1	2.07 (2.23−2.07)	271666 (23225)	38629 (6972)	97.8 (89.9)	8.8 (1.9)	7.0 (3.3)	7.5 (23.3)	0.175 (0.242)	0.236 (0.270)	0.010	1.30	24.5
βY35A	1Y31	97.2	99.2	65.9	2.13 (2.29−2.13)	247658 (19737)	35285 (6173)	97.2 (86.7)	7.2 (1.7)	6.8 (3.2)	11.2 (25.0)	0.168 (0.231)	0.251 (0.292)	0.012	1.55	24.3
βY35F	1Y35	97.3	99.4	65.9	2.12 (2.28−2.12)	239553 (20296)	36200 (6518)	97.9 (89.4)	9.7 (2.2)	6.6 (3.1)	7.8 (21.1)	0.176 (0.243)	0.244 (0.287)	0.010	1.30	23.8
βP36A	1Y45	96.9	99.0	66.0	1.99 (2.13−1.99)	267959 (23326)	43038 (7489)	96.8 (85.8)	10.9 (2.2)	6.2 (3.1)	5.2 (20.5)	0.177 (0.225)	0.209 (0.270)	0.016	1.60	23.2
βW37Y	1Y46	97.2	99.4	66.1	2.22 (2.39−2.22)	234062 (18671)	31603 (5691)	97.8 (89.6)	5.6 (1.4)	7.4 (3.3)	11.1 (27.5)	0.187 (0.258)	0.248 (0.329)	0.019	1.78	17.7
βW37H[d]	1Y4B	96.8	98.6	66.1	2.10 (2.29−2.10)		36155 (7035)	95.4 (87.6)				0.191 (0.258)	0.238 (0.317)	0.019	1.87	20.0
βW37A	1Y4F	96.8	99.2	66.2	1.99 (2.14−1.99)	265817 (23376)	42934 (7548)	97.1 (86.9)	9.8 (1.8)	6.2 (3.1)	6.5 (23.2)	0.181 (0.244)	0.216 (0.280)	0.016	1.59	24.4
βW37G	1Y4G	96.4	99.3	66.3	1.93 (2.07−1.93)	268927 (23025)	44737 (7177)	91.7 (75.7)	10.2 (1.4)	6.0 (3.2)	8.6 (29.5)	0.199 (0.322)	0.235 (0.350)	0.017	1.69	25.8
βW37E	1Y4P	96.7	99.1	66.3	1.98 (2.14−1.98)	267181 (22904)	43340 (7440)	96.7 (84.2)	8.5 (1.4)	6.2 (3.1)	7.9 (27.6)	0.192 (0.286)	0.231 (0.323)	0.018	1.74	25.2
βF42A	1Y4Q	97.2	99.3	65.8	2.11 (2.28−2.11)	250336 (21174)	36185 (6406)	97.4 (87.4)	8.8 (1.8)	6.9 (3.3)	7.4 (24.0)	0.178 (0.247)	0.245 (0.300)	0.010	1.30	24.4
βF45A	1Y4R	97.3	99.8	65.8	2.22 (2.39−2.22)	236847 (19020)	31475 (5594)	97.5 (88.2)	6.7 (1.6)	7.5 (3.4)	9.1 (25.4)	0.169 (0.230)	0.246 (0.301)	0.010	1.30	24.1
βC93A	1Y4V	97.0	99.0	65.8	1.84 (1.98−1.84)	194050 (17257)	50522 (7568)	90.8 (68.8)	11.2 (1.6)	3.8 (2.3)	6.6 (23.9)	0.180 (0.265)	0.231 (0.262)	0.011	1.40	24.3
βL96A	1Y5F	97.2	99.3	65.8	2.14 (2.31−2.14)	273130 (23347)	35049 (6371)	98.1 (90.7)	10.8 (2.5)	7.8 (3.7)	9.0 (20.6)	0.173 (0.224)	0.243 (0.286)	0.011	1.50	24.1
βH97A	1Y5J	97.1	98.6	65.9	2.03 (2.18−2.03)	467750 (36648)	40403 (7057)	97.1 (85.9)	7.9 (1.9)	11.6 (5.2)	10.1 (28.7)	0.181 (0.250)	0.245 (0.256)	0.010	1.40	24.5
βD99A	1Y5K	97.5	99.9	66.0	2.20 (2.38−2.20)	144064 (5275)	26819 (2292)	80.3 (34.1)	9.2 (3.1)	5.4 (2.3)	6.9 (22.2)	0.161 (0.227)	0.204 (0.288)	0.023	2.06	29.0
βP100A	1Y7C	97.1	100.2	65.4	2.10 (2.27−2.10)	99194 (16025)	34509 (6226)	91.2 (81.4)	12.2 (3.9)	2.9 (2.6)	4.6 (17.5)	0.207 (0.385)	0.284 (0.409)	0.013	1.40	24.5
βP100G	1Y7D	97.0	99.6	65.5	1.90 (2.05−1.90)	141212 (21688)	46698 (8500)	92.6 (82.8)	11.2 (2.3)	3.0 (2.6)	5.2 (28.4)	0.204 (0.363)	0.250 (0.302)	0.013	1.40	24.5
βN102A	1Y7G	97.2	99.5	65.6	2.10 (2.27−2.10)	95424 (16343)	34634 (6471)	91.6 (84.0)	8.4 (2.4)	2.8 (2.4)	8.4 (30.2)	0.186 (0.266)	0.259 (0.299)	0.010	1.40	23.2
βN108A	1Y7Z	97.3	99.3	65.9	1.98 (2.13−1.98)	245178 (21745)	43442 (7525)	96.4 (84.6)	11.3 (2.1)	5.6 (2.9)	6.1 (19.0)	0.176 (0.234)	0.233 (0.245)	0.010	1.30	23.6
βY145G	1Y83	97.2	99.5	65.9	1.90 (2.05−1.90)	158151 (17753)	45165 (6563)	88.9 (63.7)	17.8 (6.8)	3.5 (2.7)	3.4 (9.6)	0.195 (0.275)	0.248 (0.265)	0.011	1.30	23.5
desHis146β	1Y85	97.1	99.1	66.0	2.13 (2.29−2.13)	247179 (21588)	35576 (6440)	97.9 (90.1)	7.4 (2.0)	6.9 (3.4)	9.0 (22.4)	0.169 (0.247)	0.237 (0.267)	0.011	1.40	24.4
αR92A·4O_2·2.2 mM IHP	1Y8W	95.4	98.5	67.0	2.90 (3.13−2.90)	35018 (6374)	13441 (2570)	92.9 (87.6)	3.5 (2.5)	2.6 (2.5)	15.5 (34.0)	0.179 (0.207)	0.267 (0.354)	0.019	1.88	32.8
αY140F·4O_2·2.2 mM IHP	1YDZ	95.6	98.6	67.1	3.30 (3.56−3.30)	25981 (4609)	9186 (1735)	92.3 (85.9)	5.8 (2.8)	2.8 (2.7)	11.4 (24.1)	0.127 (0.145)	0.307 (0.390)	0.010	1.30	20.7
βV33A·4O_2·2.2 mM IHP	1YE0	96.6	99.2	66.6	2.50 (2.70−2.50)	67474 (11434)	21432 (4098)	94.8 (89.7)	5.9 (2.4)	3.1 (2.8)	10.8 (29.4)	0.184 (0.250)	0.264 (0.363)	0.024	1.88	43.8
βY35A·4O_2·2.2 mM IHP[e]	1YE1	96.4	98.9	66.9	4.50 (4.86−4.50)	13797 (2804)	3992 (792)	96.9 (95.8)	1.3 (0.8)	3.5 (3.5)	30.5 (48.9)	0.295 (0.300)	0.343 (0.307)	0.012	1.55	24.3
βY35F·4O_2·2.2 mM IHP	1YE2	96.9	99.2	66.0	1.80 (1.94−1.80)	160654 (22907)	53347 (9087)	89.6 (74.9)	12.9 (3.6)	3.0 (2.5)	4.6 (23.5)	0.176 (0.282)	0.212 (0.290)	0.019	1.55	23.2
βP36A·4O_2·2.2 mM IHP	1YEN	95.5	98.4	67.2	2.89 (3.02−2.80)	33630 (5892)	14191 (2679)	88.5 (82.8)	4.3 (2.1)	2.4 (2.2)	13.8 (32.0)	0.175 (0.232)	0.267 (0.404)	0.024	2.01	47.2
βW37A·4O_2·0mM IHP	1YEO	95.9	98.9	66.8	2.22 (2.39−2.22)	236825 (18227)	31225 (5495)	97.3 (87.1)	9.3 (2.1)	7.6 (3.3)	7.0 (22.2)	0.180 (0.224)	0.228 (0.259)	0.026	1.47	25.6
βW37A·4O_2·2.2mM IHP	1YIE	96.2	99.0	66.8	2.40 (2.58−2.40)	121947 (16577)	24954 (4549)	97.1 (90.4)	7.2 (1.6)	4.9 (3.6)	10.7 (28.1)	0.185 (0.236)	0.273 (0.309)	0.010	1.40	27.2
βW37Y·4O_2·0mM IHP	1YEQ	96.2	99.6	67.0	2.75 (2.96−2.75)	90981 (12649)	17171 (3230)	98.9 (94.9)	5.5 (1.5)	5.3 (3.9)	17.1 (30.1)	0.196 (0.248)	0.274 (0.338)	0.027	1.34	22.3
βW37G·4O_2·0mM IHP	1YEU	96.3	99.2	66.9	2.12 (2.28−2.12)	241109 (19160)	35935 (6288)	96.7 (86.1)	9.6 (1.1)	6.7 (3.0)	8.2 (29.6)	0.201 (0.276)	0.254 (0.309)	0.033	1.78	30.3
βW37H·4O_2·2.2mM IHP	1YG5	95.6	98.6	66.8	2.70 (2.92−2.70)	53259 (6695)	16452 (2690)	92.1 (74.6)	4.3 (2.7)	3.2 (2.5)	11.1 (24.8)	0.179 (0.266)	0.273 (0.390)	0.027	2.48	33.0
βW37E·4O_2·0mM IHP	1YEV	96.1	99.3	67.1	2.11 (2.27−2.11)	252494 (21302)	36695 (6536)	97.6 (88.5)	9.2 (1.6)	6.9 (3.3)	8.3 (27.3)	0.194 (0.256)	0.242 (0.288)	0.030	1.71	27.9
βW37E·4NO·0mM IHP	1RQA	95.3	97.8	66.8	2.11 (2.27−2.11)	236515 (16855)	35916 (6537)	98.0 (90.5)	9.6 (2.0)	6.6 (2.6)	8.5 (23.1)	0.188 (0.234)	0.231 (0.274)	0.023	2.33	26.2

Table 1 (Continued)

hemoglobin[b]	PDB code	*a* (Å)	*b* (Å)	*c* (Å)	resolution (Å)	total measurements	unique reflns	completeness (%)	av $I/\sigma(I)$	av multiplicity	R_{merge} (%)	R_{cryst} [c]	R_{free} [c]	rms bond lengths (Å)	rms bond angles (deg)	av *B* factor (Å^2)
βW37E(αZn)·2O_2·0mM	1YGD	96.3	99.1	66.8	2.73 (2.94−2.73)	97735 (13543)	17254 (3138)	97.9 (90.5)	5.0 (1.5)	5.7 (4.3)	13.4 (30.1)	0.190 (0.249)	0.266 (0.325)	0.019	1.38	22.9
βH97A·4O_2·2.2 mM IHP	1YGF	96.6	98.3	66.1	2.70 (2.92−2.70)	41794 (7108)	16077 (2951)	90.2 (81.6)	8.5 (3.0)	2.6 (2.4)	8.3 (24.1)	0.164 (0.195)	0.273 (0.397)	0.026	1.73	34.4
βP100A·4O_2·2.2 mM IHP	1YIH	96.9	99.5	65.6	2.00 (2.16−2.00)	98987 (14876)	38030 (6877)	87.7 (77.7)	12.7 (5.2)	2.5 (2.2)	4.6 (13.4)	0.183 (0.255)	0.247 (0.233)	0.011	1.50	23.9
HbA·4O_2·2.2 mM IHP	1YH9	97.1	99.6	66.1	2.20 (2.37−2.20)	95276 (23737)	31525 (8798)	93.7 (87.7)	4.7 (3.3)	3.1 (2.7)	7.3 (26.6)	0.189 (0.254)	0.236 (0.312)	0.013	1.26	30.5
HbA·4O_2·5.0 mM IHP	1YHE	96.9	99.2	66.1	2.10 (2.27−2.10)	122314 (12458)	32696 (4049)	87.1 (61.2)	10.6 (5.0)	3.7 (3.1)	5.5 (13.6)	0.167 (0.179)	0.208 (0.243)	0.021	1.49	23.8
HbA·4O_2·10.0 mM IHP	1YHR	95.2	98.4	66.5	2.60 (2.80−2.60)	60525 (10503)	18673 (3549)	94.7 (89.0)	7.3 (3.3)	3.2 (3.0)	9.3 (20.8)	0.175 (0.199)	0.270 (0.341)	0.021	1.88	23.4

[a] The values in parentheses are for the highest resolution data shell. [b] The hemoglobin notation for the liganded structures has the form hemoglobin variant·ligation state·IHP concentration. [c] For structures that were subjected to the $R_{free}^{local-5}$ analysis (see Materials and Methods), R_{cryst} and R_{free} are for the refinement in which the "zero" test set was omitted from the refinement. [d] Although data collection statistics are not available for βW37H because the unprocessed diffraction images were lost due to a computer hard drive failure, the quality of the data is comparable to other 2.1 Å data sets. [e] The βY35A·4O_2·2.2 mM IHP atomic model was subjected only to rigid-body refinement.

each tetramer are averaged about the dyad axis. Then a "sieve-fit" iterative least-squares superposition similar to that described by Gerstein and Chothia (*20*, *48*) is used to superimpose the $\alpha1\beta1$ dimers of a pair of hemoglobin tetramers and to identify the backbone atoms of the $\alpha1\beta1$ "static core". As a global measure of the magnitude of a quaternary structure difference, the parameter Δ_Q is defined as the rms deviation of the backbone atoms of the non-superimposed $\alpha2\beta2$ static core. Next, the $\alpha2\beta2$ dimers are superimposed, and the set of screw-rotation parameters associated with this second superposition describes the magnitude and direction of the dimer−dimer rotation. Only four independent parameters are required to uniquely specify the screw-rotation transformation for dimer−dimer rotation (*47*): one direction angle of the screw rotation axis (α or γ), the *y*-intercept (y_{int}) of the screw rotation axis, the magnitude of rotation (ρ_{rot}), and the translation distance (τ).

The intradimer rigid-body rotation was determined in a similar manner. First the "sieve-fit" superposition was used to superimpose the $\beta1$ subunits of a pair of hemoglobin $\alpha1\beta1$ dimers and to identify the backbone atoms of the $\beta1$ static core. Then the $\alpha1$ subunits were superimposed, and the set of screw-rotation parameters associated with this second superposition describes the magnitude and direction of intradimer rotation. The main parameter of interest in this case is the magnitude of intradimer rotation, referred to below as the intradimer bending angle (ρ_{bend}).

To identify oxygen-induced changes in tertiary structure, corresponding subunits of the deoxy and oxygenated structures were superimposed using the sieve-fit procedure. Concerted changes in tertiary structure were identified by calculating δ_5 plots as previously described (*20*). In addition, the rms deviation of all the atoms (backbone plus side chain atoms) was calculated for each pair of corresponding pentapeptides in the superimposed subunits. This statistic, referred to as $rmsd_5$, is plotted versus residue number to generate a profile of the five-residue-averaged tertiary structure changes. A five-residue window was selected so that the δ_5 and $rmsd_5$ values corresponded with the $\langle R_{free}^{local-5} \rangle$ values (above).

RESULTS

Mutation-Induced Quaternary Structure Transitions: Interdimer Rotation. Rigid-body analysis of mutation-induced $\alpha1\beta1/\alpha2\beta2$ interdimer rotation is shown in Table 2, where the entries are sorted on the absolute value of the interdimer rotation angle ρ_{rot}, which varies from 0° to 2.1°. Table entries are color-coded according to the ratio of the mutant to wild-type CO-combination rate constants as reported by Noble el al. (*14*). The ratio Δ_Q/σ (i.e. the ratio of the rms deviation of the non-superimposed $\alpha2\beta2$ static core to the rms deviation of the superimposed $\alpha1\beta1$ static core) is a measure of the significance of the interdimer rotation angle ρ_{rot}.

The βP100G and βP100A mutations clearly induce significant interdimer rotations with rotation magnitudes of 2.1° and 1.3° and Δ_Q/σ values of 7.1 and 5.5, respectively. But these mutation-induced transitions have screw-rotation axes that appear be unique to this residue. On the other hand, the mutation-induced $\alpha1\beta1/\alpha2\beta2$ interdimer rotations associated with the βW37G, βW37E, desArg141α, βW37A, βP36A, and βW37Y mutations reflect a more general and

Table 2: Mutation-Induced Quaternary Structure Transitions[a]

Transition	α (deg.)	y_{int} (Å)	ρ_{rot} (deg.)	σ (A)	Δ_Q (Å)	Δ_Q/σ
βV1M → βP100G	96.3°	10.4	2.1°	0.12	0.85	7.1
βV1M → βW37G	104.3°	-12.9	2.0°	0.13	0.88	6.8
βV1M → βW37E	108.6°	-16.7	1.5°	0.13	0.74	5.7
βV1M → βP100A	103.1°	14.6	1.3°	0.11	0.60	5.5
HbA → desArg141α	117.2°	-8.3	1.0°	0.08	0.38	4.8
βV1M → βW37A	102.7°	-17.7	0.9°	0.11	0.46	4.2
βV1M → βP36A	104.5°	-8.9	0.8°	0.07	0.33	4.7
βV1M → βW37Y	109.3°	-17.8	0.6°	0.12	0.29	2.4
HbA → desHis146β	76.9°	-6.0	0.6°	0.06	0.18	3.0
HbA → αR92A	91.0°	6.2	-0.6°	0.13	0.30	2.3
HbA → αY140A	177.7°	-17.8	0.5°	0.11	0.26	2.4
βV1M → βD99A	100.7°	11.0	-0.5°	0.12	0.26	2.2
βV1M → βY145G	134.5°	12.9	-0.4°	0.07	0.18	2.6
βV1M → βW37H	109.2°	-20.7	0.4°	0.12	0.22	1.9
βV1M → βC93A	89.2°	9.4	0.4°	0.05	0.16	3.2
βV1M → βN102A	22.4°	15.0	-0.3°	0.06	0.16	3.7
HbA → αY42A	160.8°	-39.2	0.3°	0.13	0.30	2.3
βV1M → βH97A	89.1°	-12.6	0.3°	0.10	0.21	2.1
βV1M → βL96A	85.0°	2.1	0.3°	0.05	0.12	2.4
HbA → αN97A	159.1°	-20.5	-0.3°	0.12	0.18	1.5
HbA → αY140F	93.3°	-21.2	0.2°	0.08	0.19	2.4
HbA → αL91A	173.9°	-21.1	0.2°	0.05	0.11	2.2
HbA → αD94G	142.5°	39.3	0.2°	0.10	0.22	2.2
HbA → αP95A	125.6°	-24.4	0.2°	0.05	0.13	2.6
βV1M → βV34G	64.2°	-25.2	0.2°	0.06	0.13	2.2
βV1M → βF42A	112.1°	31.5	0.1°	0.04	0.08	2.0
βV1M → βY35F	93.1°	-21.4	0.1°	0.04	0.07	1.8
βV1M → βF45A	16.2°	-33.5	0.1°	0.05	0.09	1.8
βV1M → βY35A	63.8°	-27.9	0.1°	0.06	0.08	1.3
βV1M → βN108A	163.0°	-37.4	0.0°	0.05	0.06	1.2
HbA → αK40G	160.4°	-194.9	0.0°	0.07	0.13	1.9
βV1M → βV33A	7.0°	59.9	0.0°	0.06	0.11	1.8

[a] The entries in this table are color-coded according to the ratio of the mutant to wild-type CO-combination rate constants as reported by Noble el al. (*14*) as follows: red >5, orange 2.6−5, green 1.6−2.5, and light blue 0.7−1.5. Entries in black display heterogeneous CO-combination kinetics in the presence of IHP (see Noble et al. (*14*)). The screw-rotation translation (τ) has not been included in this table because it is very close to zero for all these transitions.

fundamental mode of relaxing the quaternary constraints imposed by the Trp37β cluster. These six mutation-induced transitions have very similar screw-rotation axes (with an average α direction angle of 108° (± 5°) and an average y-intercept of −13.7 Å (± 4.4 Å)), positive screw-rotation angles that vary from +0.6° to +2.0°, and large Δ_Q/σ values that vary from 2.4 to 6.8. Moreover, since the mutations associated with the three residues Arg141α, Pro36β, and Trp37β all disrupt quaternary constraints in the Trp37β cluster and result in high ligand-affinity structures (as indicated by the color-coding in Table 2), we refer to them as T_{High} structures and the rigid-body transitions as T-to-T_{High} transitions. All the other mutations listed in Table 2 (those below the thick line) induce transitions with small rotation magnitudes (−0.5° to +0.6°), lower Δ_Q/σ values, and more or less randomly oriented and positioned screw-rotation axes.

The fact that six mutations of three residues resulted in very similar screw-rotation transitions could be a coincidence. However, as discussed below, ligand binding also induces very similar α1β1/α2β2 screw-rotation transitions. That is, breaking quaternary constraints in the Trp37β cluster by mutation or by ligation induces the same quaternary relaxation.

Ligation-Induced Quaternary Structure Transitions in the β37 Mutants: Interdimer Rotation. When crystals of wild-type deoxyhemoglobin are exposed to atmospheric oxygen at room temperature, they disorder and the X-ray diffraction

Table 3: Ligand-Induced Quaternary Structure Transitions in 37β Hemoglobin Mutants[a]

T-to-T_{High} Transition	Interdimer Rotation						Intradimer Bending
	α	y_{int} (Å)	ρ_{rot}	σ (Å)	Δ_Q (Å)	Δ_Q/σ	ρ_{bend}
T → βW37E•4O_2•0mM IHP	105.1°	-13.5	5.6°	0.30	2.44	8.1	2.3°
T → βW37A•4O_2•0mM IHP	109.2°	-13.8	5.1°	0.22	2.24	10.2	2.1°
T → βW37Y•4O_2•0mM IHP	103.3°	-13.4	5.0°	0.31	2.19	7.1	1.9°
T → βW37G•4O_2•0mM IHP	114.9°	-16.9	4.5°	0.23	2.13	9.3	2.1°
T → βW37A•4O_2•2.2mM IHP	102.8°	-11.2	5.6°	0.26	2.30	8.9	2.1°
T → βW37H•4O_2•2.2mM IHP	106.2°	-13.0	4.8°	0.39	2.16	5.5	2.2°
T → βW37E(αZn)•2O_2•0mM IHP	115.1°	-16.1	4.0°	0.22	1.91	8.7	1.9°
T → βW37E•4NO•0mM IHP	113.5°	-10.7	6.0°	0.38	2.42	6.4	2.9°

[a] The entries in this table are color-coded according to the ratio of the mutant to wild-type CO-combination rate constants as reported by Noble el al. (*14*) as follows: red >5, orange 2.6−5, green 1.6−2.5, and light blue 0.7−1.5. The screw-rotation translation (τ) has not been included in this table because it is very close to zero for all the T-to-T_{High} transitions.

Table 4: Ligand-Induced Quaternary Structure Transitions in Wild-Type Hemoglobin and Non-37β Hemoglobin Mutants[a]

T-to-T_{High} Transition	Interdimer Rotation						Intradimer Bending
	α (deg.)	y_{int} (Å)	ρ_{rot} (deg.)	σ (A)	Δ_Q (Å)	Δ_Q/σ	ρ_{bend} (deg.)
T → βP36A•4O_2•2.2mM IHP	108.7°	-14.3	5.9°	0.38	2.65	7.0	2.8°
T → αY140F•4O_2•2.2mM IHP	110.4°	-16.0	5.3°	0.28	2.57	9.1	2.9°
T → αR92A•4O_2•2.2mM IHP	113.9°	-13.7	5.1°	0.46	2.26	4.9	3.0°
T → βY35A•4O_2•2.2mM IHP	105.2°	-12.7	4.6°	0.31	2.00	6.5	2.4°
T → βV33A•4O_2•2.2mM IHP	106.9°	-13.3	2.3°	0.28	1.05	3.8	1.1°
T → βH97A•4O_2•2.2mM IHP	126.0°	-6.7	1.4°	0.27	0.59	2.2	1.2°
T → βP100A•4O_2•2.2 mM IHP	125.5°	-12.9	1.3°	0.21	0.69	3.3	1.1°
T → βY35F•4O_2•2.2mM IHP	117.6°	-9.6	0.9°	0.15	0.38	2.5	0.9°
T → HbA•4$O_2$2.2mM IHP	122.4°	-11.6	0.6°	0.15	0.30	2.0	0.9°
T → HbA•4O_2•5.0mM IHP	120.2°	-8.0	0.7°	0.13	0.29	2.2	0.8°
T → HbA•4O_2•10.0mM IHP	116.9°	-10.8	4.3°	0.36	1.81	5.0	2.4°
T → rHb1.1•Fe^{+3}4CN•0mM IHP	112.0°	-14.8	8.6°	0.40	3.79	9.5	3.6°

[a] The entries in this table are color-coded according to the ratio of the mutant to wild-type CO-combination rate constants as reported by Noble el al. (*14*) as follows: red >5, orange 2.6−5, green 1.6−2.5, and light blue 0.7−1.5. The screw-rotation translation (τ) has not been included in this table because it is very close to zero for all the T-to-T_{High} transitions.

pattern becomes useless for X-ray data collection. In contrast, crystals of the deoxyhemoglobin β37 mutants can be exposed to air at room temperature without disordering. Electron density images show that diatomic oxygen is bound to all four heme groups in these crystals, and rigid-body screw-rotation analysis (for the four β37 entries in Table 3) shows that the ligation-induced transitions have very similar screw-rotation axes (the average α direction angle is 108° (±5°) and the average *y*-intercept is −14.4 Å (±1.5 Å)) and positive screw-rotation angles that vary from +4.5° to +5.6°. Moreover, these ligand-induced screw-rotation axes are very similar to the mutation-induced screw-rotation axes described above. That is, when crystals of the deoxyhemoglobin β37 mutants are exposed to air, oxygen binding induces further rotation about a T-to-T_{High} screw-rotation axis. As indicated in the $[\alpha(Zn^{+2})\beta W37E(Fe^{+2}\text{-}O_2)]_2$ structure (referred to as βW37E(αZn)•2O_2•0 mM IHP in Table 3), the same is true when ligand is bound to only the β subunits. A T-to-T_{High} transition also is observed in the βW37E•4NO•0 mM IHP structure, but in this case the screw-rotation magnitude is slightly larger than it is in βW37E•4O_2•0 mM IHP.

Ligation-Induced Quaternary Structure Transitions in Wild-Type Hemoglobin and in the Non-β37 Mutants: Interdimer Rotation. Crystals of the other deoxyhemoglobin mutants (i.e., the non-β37 mutants) behave like wild-type deoxyhemoglobin crystals in that they disorder when exposed to air at room temperature and, therefore, are not useful for X-ray diffraction experiments. Since Paoli et al. (*29*) found that, at 4 °C and in the presence of IHP, wild-type deoxyhemoglobin crystals can bind oxygen without disordering, a similar approach was applied to study ligand-induced transitions in mutant hemoglobin crystals. The results from these experiments (Table 4) fall into two groups with slightly different screw-rotation axes. The transitions in the first group (the first five entries in Table 4) all involve residues that are part of the Trp37β cluster and have high ligand affinity

as indicated by the color-coding in Table 4 (except for Val33β which is located on the edge of the cluster). The ligation-induced transitions associated with the first group have very similar screw-rotation axes (i.e., an average α direction angle of 108° (±4°) and an average *y*-intercept of −13.9 Å (±1.2 Å)) that are spatially close to the T-to-T_{High} rotation axes observed for the deoxy Trp37β cluster mutants and the liganded 37β mutants. The screw-rotation angles for the first group vary from +2.3° to +5.9°.

The second group consists of only three mutant hemoglobins and wild-type hemoglobin. Two of the mutants, βH97A and βP100A, are not part of the Trp37β cluster and have normal ligand affinity (as indicated by the color-coding in Table 4). Although the third mutant, βY35F, is within the Trp37β cluster, it is a conservative mutation that does not greatly disrupt quaternary constraints since its CO-combination rate is the same as that of wild-type hemoglobin (*49*). The second group has ligation-induced transitions with very similar screw-rotation axes (an average α direction angle of 123° (±5°) and an average *y*-intercept of −9.7 Å (±3.0 Å)) that are significantly different from the first group. The ligation-induced rotation angles for wild-type hemoglobin and for the three mutants in the second group vary from +0.6° to +1.4°, which is significantly smaller than those of the first group. It is interesting to note that, for one member of this second group, βP100A, the ligation-induced transition is about the wild-type screw-rotation axis even through the mutation-induced transition (see above) is about a very different axis.

The T-to-T_{High} Screw-Rotation Axes Are Independent of the Crystal Lattice. It is possible that the similarity of the T-to-T_{High} screw-rotation axes observed for the mutation- and ligand-induced quaternary structure changes is the result of the common crystal lattice used in the experiments described above. However, our analysis of a fully liganded structure previously reported by Kroeger and Kundrot (*50*) indicates that this is not the case. This crystal structure, referred to as the B-state by Kroeger and Kundrot, is of the cyanomet form of rHb1.1. (rHb1.1 is a recombinant hemoglobin, containing the mutation βN108K, in which the COOH-terminus of the α1 subunit is cross-linked to the NH_2-terminus of the α2 subunit by a glycine bridge.) Importantly, cyanomet rHb1.1 was crystallized in a space group that is different from the low-salt crystal form of hemoglobin used in the experiments reported in this paper. As shown in Table 4, our analysis of this structure shows that the B-state is a T_{High} tetramer with a T-to-T_{High} screw-rotation axis that falls within the range of the axes in the first group of IHP stabilized T_{High} structures described above but with a rotation magnitude that is significantly larger ($\rho_{rot} = 8.6°$). Therefore, we can conclude that the T-to-T_{High} transitions are an inherent property of the hemoglobin tetramer.

The Influence of IHP on Ligand-Induced Interdimer Rotation. The fact that very similar T-to-T_{High} rotation axes are observed when the 37β mutants are exposed to air and when the IHP stabilized non-β37 mutants are exposed to oxygen implies that IHP does not greatly influence the direction of the T-to-T_{High} transition. Further evidence of this conjecture was obtained by determining the ligand-induced screw-rotation axis for the βW37A−IHP complex exposed to air at room temperature and for the βW37H−IHP complex exposed to oxygen at −4 °C. In the case of the βW37A−IHP complex the screw-rotation parameters were $\alpha = 102.8°$, $y = -11.2$ Å, $\rho_{rot} = 5.6°$, and in the case of the βW37H−IHP complex the screw-rotation parameters were $\alpha = 106.2°$, $y = -13.0$ Å, $\rho_{rot} = 4.8°$. From these data, it is clear that IHP does not greatly influence the direction of the T-to-T_{High} transition. However, from the results presented below it is clear that IHP can influence the magnitude of the T-to-T_{High} transition in crystalline hemoglobin.

Experiments were carried out to determine the influence of IHP concentration on the T-to-T_{High} transition in wild-type hemoglobin. Specifically, crystals of wild-type hemoglobin were soaked in the substitute mother liquor that contained either 5 mM IHP, 10 mM IHP, or 20 mM IHP (instead of 2.2 mM as in the above experiments) and exposed to oxygen. A diffraction data set collected at −4 °C on a crystal soaked in 5 mM IHP revealed a T-to-T_{High} transition that is essentially identical to that observed at 2.2 mM IHP (Table 4). In contrast, a larger ligand-induced T-to-T_{High} transition was observed for the crystal soaked in 10 mM IHP (Table 4). Specifically, increasing the IHP concentration to 10 mM changed the direction of the T-to-T_{High} screw-rotation axis by −10° and increased ρ_{rot} from 0.6° to 4.3°, making it more similar to the ligand-induced T-to-T_{High} transitions observed for the Trp37β cluster mutants (see Table 4). The reason for the large increase in the magnitude of the T-to-T_{High} transition is not clear. It may be due to increased IHP occupancy at the organic phosphate binding site (although no increase in electron density at the IHP binding site was evident), or it may be that the increase in ionic strength caused by the highly charged IHP molecule weakened lattice constraints and allowed a larger T-to-T_{High} transition to occur. When crystals soaked in 20 mM IHP were exposed to oxygen, the diffraction pattern degraded dramatically, making it impossible to collect usable diffraction data. This result is consistent with the possibility that high IHP concentrations weaken the lattice constraints.

Mutation- and Ligation-Induced Changes in $\alpha\beta$ Dimer Quaternary Structure: Intradimer Bending. In the initial comparison of liganded and deoxy horse hemoglobin, Perutz et al. (*51*) noted the following: "In the transition from oxy to deoxyhaemoglobin, movement in the contact $\alpha1\beta1$ is slight; relative to the α1 subunit, the β1 subunit rotates by 3.7° about a screw axis and moves by 0.3 Å along it." However, they felt that the functional importance of this bending motion was unclear. To the best of our knowledge, this bending motion has never been mentioned in any subsequent publications analyzing hemoglobin structure. In fact, most subsequent analyses of ligand-induced structural changes in hemoglobin have treated the $\alpha\beta$ dimer as a rigid structure that does not change upon ligand binding (*46*, *52*).

We have carried out rigid-body screw-rotation analyses of intradimer bending for all the ligation-induced T-to-T_{High} transitions as well as for the T-to-R and T-to-R2 transitions. We find that $\alpha\beta$ dimer bending is associated with all these transitions with magnitudes (ρ_{bend}) that vary from 0.8° to 3.9°. The largest bending magnitudes, 3.7° and 3.9°, occur for the T-to-R and T-to-R2 transitions, respectively. (The T-to-R value is in excellent agreement with Perutz's initial measurement on liganded and deoxy horse hemoglobin (*51*).) With regard to the ligand-induced T-to-T_{High} transitions, the $\alpha\beta$ dimer bending magnitudes (Tables 3 and 4) range from 0.8° (in wild-type crystals soaked in 2.2 mM IHP) to 3.6° (in

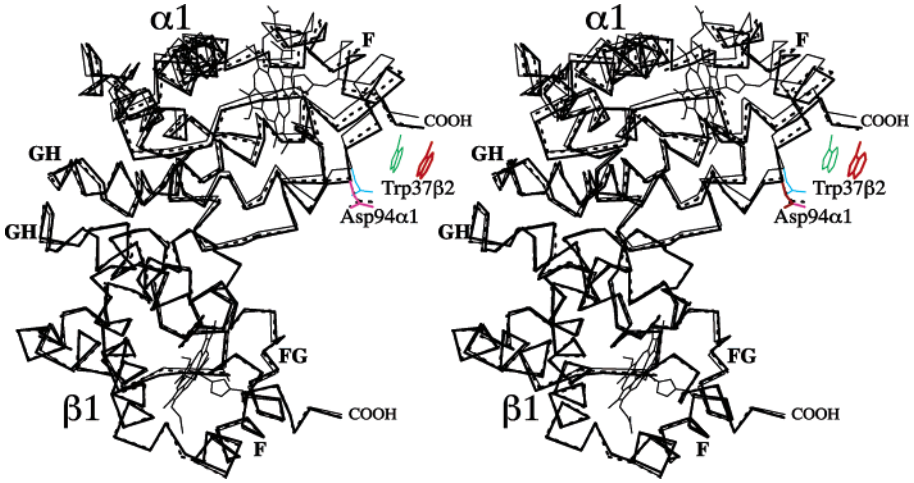

FIGURE 2: Stereodiagram showing α-carbon tracings of the α1β1 dimers of βW37E(αZn)·2O_2·0 mM IHP (dashed lines) and αR92A·4O_2·2.2 mM IHP (thick lines) after they have been superimposed on the β1 subunit of wild-type deoxyhemoglobin (thin lines) using the sieve-fit procedure. The displacements of the βW37E(αZn)·2O_2·0 mM IHP and αR92A·4O_2·2.2 mM IHP α1 subunits relative to the wild-type α1 subunit represent 1.9° and 3.0° of ligand-induced intradimer bending, respectively. In the case of βW37E(αZn)·2O_2·0 mM IHP the intradimer bending is associated with ligand binding to only the β subunits, since the α subunits cannot bind oxygen. The side chain of Asp94α1 is shown for deoxyhemoglobin, βW37E(αZn)·2O_2·0 mM IHP, and αR92A·4O_2·2.2 mM IHP (light blue, dashed, and magenta, respectively), and the side chain of Trp37β2 is shown for deoxyhemoglobin (green) and for αR92A·4O_2·2.2 mM IHP (red). The bending motion alone (i.e., in the absence of interdimer rotation) is capable of disrupting interactions in the Trp37β2 cluster, which can be seen as the movement of Asp94α1 in βW37E(αZn)·2O_2·0 mM IHP (dashed) and in αR92A·4O_2·2.2 mM IHP (magenta) away from the side chain of Trp37β2 in deoxyhemoglobin (green). In the absence of interdimer rotation, intradimer bending also creates close contacts of less than 2 Å between Trp37β2 (green) and the main chain of Arg92α1. Interdimer rotation relieves this steric clash as Trp37β2 (red) moves away from the α1 subunit.

cyanomet rHb1.1). Rigid-body analysis of the deoxy mutants shows that intradimer bending also occurs in mutants in which there is interdimer rotation about a T-to-T_{High} screw rotation axis. Specifically, mutation-induced intradimer bending magnitudes of 0.5°, 0.6°, 0.6°, 0.9°, 1.2°, and 1.2° are observed for βP36A, βW37Y, desArg141α, βW37A, βW37E, and βW37G, respectively.

The αβ dimer bending motion occurs in T-to-T_{High} transitions in a way that can disrupt the Trp37β cluster of quaternary constraints. Intradimer dimer bending can be analyzed by superimposing (using the sieve-fit procedure) one subunit of a liganded α1β1 dimer onto the corresponding subunit of deoxyhemoglobin. Dimer bending can then displayed as the relative movement of the non-superimposed pair of subunits. This is illustrated in Figure 2 where the β1 subunits of two liganded T_{High} structures have been superimposed on the β1 subunit of deoxyhemoglobin. The displacement of the non-superimposed α1 subunits in this figure corresponds to 1.9° and 3.0° of intradimer dimer bending for βW37E(αZn)·2O_2·0 mM IHP and αR92A·4O_2·2.2 mM IHP, respectively. It is clear from Figure 2 that the αβ dimer bending motion is leveraged over the distance between the β1 heme and the FG-corner/G-helix of the α1 subunit such that residues 92α1 through 95α1 move by ~1 Å or more. This motion widens the distance and disrupts the polar interaction between Asp94α1 and Trp37β2, and in the absence of interdimer rotation, generates a steric clash (a 2.0 Å nonbonded contact) between the backbone atoms of Arg92α1 and Trp37β2. This steric clash is relieved by α1β1/α2β2 interdimer rotation.

Correlation between Interdimer Rotation and Intradimer Bending. The above analysis suggests that intradimer bending and interdimer rotation are structurally linked and should be highly correlated. This is in fact observed for all the mutation-induced and ligation-induced T-to-T_{High} transitions (Figure 3). The correlation also holds for the cyanomet rHb1.1 structure. Since cyanomet rHb1.1 was crystallized in the fully liganded form directly from solution, and in a different crystal lattice, the correlation between the magnitudes of αβ dimer bending and αβ dimer rotation also must be an intrinsic property of the hemoglobin molecule. We can conclude that the loss of quaternary constraints, either by mutation or ligation or both, results in the relaxation of the hemoglobin tetramer via the coordinated motions of interdimer rotation and intradimer bending.

Ligand-Induced α Subunit Tertiary Structure Changes Associated with T-to-T_{High} Transitions. When crystallographic methods are used to characterize small tertiary structure changes caused by mutation or the binding of ligand, a fundamental issue that should be specifically addressed is the validity of these small changes in structure. That is, it must be determined if these are genuine structural changes that are due to ligand binding or mutation, or if they are simply due to small random variations in atomic positions that are to be expected in any X-ray structure determination. One way to establish the validity of a small change in structure is to demonstrate that it occurs in two or more pairs of structures that were independently determined in the same crystal lattice (i.e., by making use of noncrystallographic symmetry) or in different crystal lattices. The $R_{free}^{local-5}$ parameter (described above) provides a second, complementary approach to the verification of small changes in tertiary structure. It has recently been used to validate small mutation-induced changes in hemoglobin tertiary structure (*53*) and tertiary structure changes induced by the binding of nitric oxide to deoxyhemoglobin crystals (*22*).

Figure 4 illustrates the detection and characterization of valid O_2-induced α subunit tertiary structure changes that are associated with the T-to-T_{High} transition in βW37A.

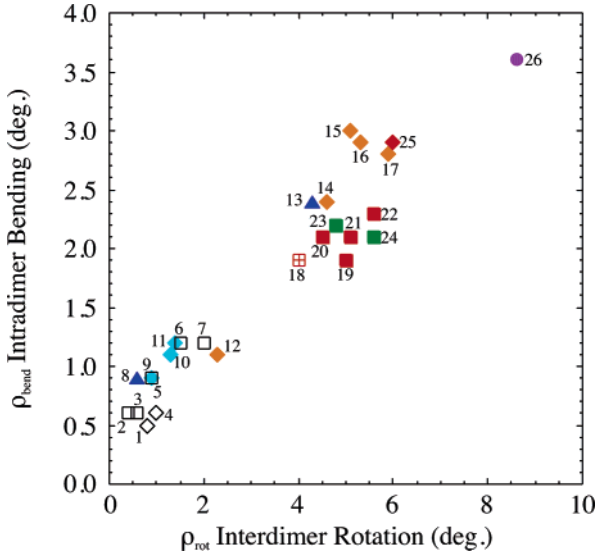

FIGURE 3: Plot showing the correlation between the magnitude of intradimer bending, ρ_{bend}, and interdimer rotation, ρ_{rot}, in the T_{High} structures. Symbols indicate mutation-induced transitions in 37β mutants (open squares), mutation-induced transitions in non-37β mutants (open diamonds), type 1 ligation-induced transitions (i.e, transitions with small ρ_{rot} values) in IHP-stabilized non-37β mutants (light blue diamonds), type 2 ligation-induced transitions (i.e., transitions with larger ρ_{rot} values) in IHP-stabilized non-37β mutants (orange diamonds), ligation-induced transitions in IHP-stabilized wild-type hemoglobin (blue triangles), ligation-induced transitions in 37β mutants (red squares), ligation-induced transitions in 37β mutants in the presence of IHP (green squares), ligation-induced transition in βW37E(αZn)·2O_2·0 mM IHP (red crossed square), ligation-induced transitions in βW37E·4NO·0 mM IHP (red diamond), and ligation-induced transitions in cyanomet rHb1.1 (purple circle). Numbers identify the T_{High} structures as follows; βP36A (1), βW37H (2), βW37Y (3), desArg141α (4), βW37A (5), βW37E (6), βW37G (7), HbA·4O_2·2.2 mM IHP (8), βY35F·4O_2·2.2 mM IHP (9), βP100A·4O_2·2.2 mM IHP (10), βH97A·4O_2·2.2 mM IHP (11), βV33A·4O_2·2.2 mM IHP (12), HbA·4O_2·10.0 mM IHP (13), βY35A·4O_2·2.2 mM IHP (14), αR92A·4O_2·2.2 mM IHP (15), αY140F·4O_2·2.2 mM IHP (16), βP36A·4O_2·2.2 mM IHP (17), βW37E(αZn)·2O_2·0 mM IHP (18), βW37Y·4O_2·0 mM IHP (19), βW37G·4O_2·0 mM IHP (20), βW37A·4O_2·0 mM IHP (21), βW37E·4O_2·0 mM IHP (22), βW37H·4O_2·2.2 mM IHP (23), βW37A·4O_2·2.2 mM IHP (24), βW37E·4NO·0 mM IHP (25), rHb1.1·Fe^{+3}4CN·0 mM IHP (26).

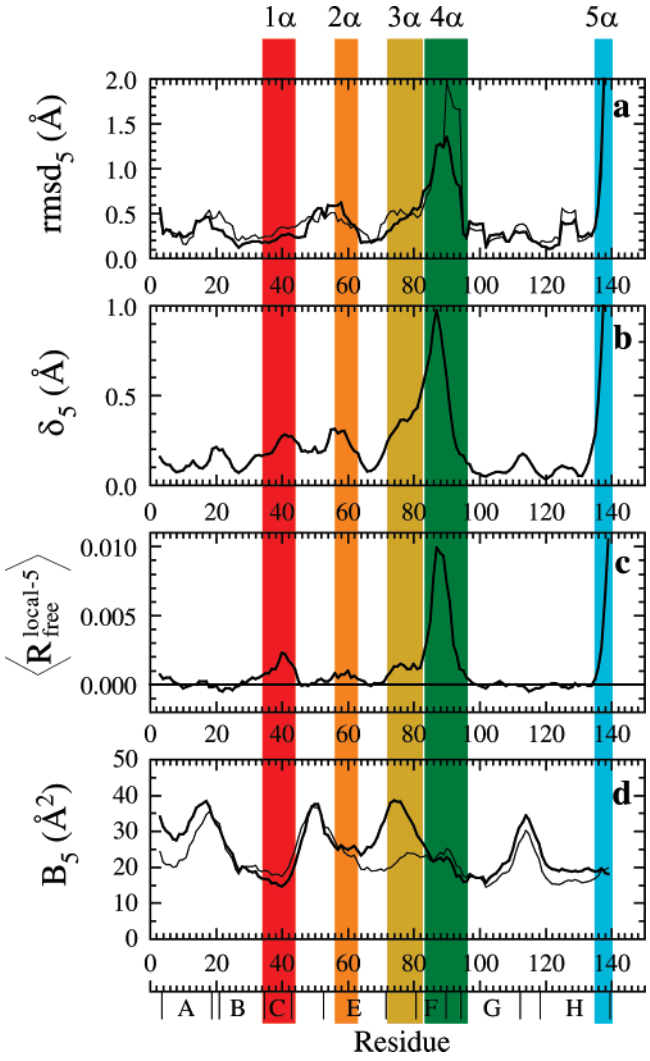

FIGURE 4: Plots of (a) rmsd$_5$, (b) average δ_5, (c) $\langle R_{free}^{local-5} \rangle$, and B_5 for the α subunits where each parameter has been calculated for all overlapping five-residue peptides. The rmsd$_5$ parameter is the root-mean-square-deviation in α subunit atomic coordinates calculated after the α subunits of βW37A·4O_2·0 mM IHP have been superimposed (using the sieve-fit procedure) on the corresponding subunits of deoxyhemoglobin. δ_5 is the magnitude of the atomic displacement vector for the backbone atoms of a five-residue peptide as defined in Kavanaugh et al. (*20*). The δ_5 profile in panel b is the average of the δ_5 profiles for the α1 and α2 subunits. $\langle R_{free}^{local-5} \rangle$ is a cross-validation statistic that is sensitive only to local changes in tertiary structure (see Materials and Methods). Positive $\langle R_{free}^{local-5} \rangle$ values identify five regions of valid changes in structure that are labeled 1α through 5α (top of figure) and highlighted by colored bars. The B_5 profiles are the average atomic temperature factors for all the atoms in a given pentapeptide of the wild-type deoxyhemoglobin α subunits. In panels a and d the α1 and α2 subunit profiles are drawn in thin and thick lines, respectively. The globin helical boundaries are indicated along the bottom axis.

Specifically, shown in Figure 4 are plots of α chain rmsd$_5$, δ_5, $\langle R_{free}^{local-5} \rangle$, and B_5 profiles (see caption) for the T-to-T_{High} transition in βW37A hemoglobin where each parameter has been calculated over all overlapping five-residue peptides. The $\langle R_{free}^{local-5} \rangle$ profile in Figure 4c was used to identify and cross-validate five regions of ligand-induced changes in α subunit tertiary structure that are labeled 1α through 5α and highlighted by color-coded bars. The largest $\langle R_{free}^{local-5} \rangle$ features, 4α and 5α, correspond to the largest peaks in the rmsd$_5$ and δ_5 profiles (Figure 4a and Figure 4b) which occur at the α F-helix/FG-corner and the α C-terminus, respectively. The structural changes in α F-helix/FG-corner stereochemistry show that the central portion of feature 4α corresponds to an α-to-π helix transition at the COOH-terminal end of the F-helix (see below). This transition results in a large shift in the position of the His87α-Ala88α dipeptide toward Tyr140α as illustrated in Figure 5 where the α1 subunits of deoxyhemoglobin and βW37A·4O_2 have been superimposed. In liganded βW37A, the steric collision between Ala88α1 and Tyr140α1 is relieved by the movement of the Tyr140α1 side chain (feature 5α) into the α1β2 interface. Specifically, the Tyr140α1 side chain moves into the area occupied by Trp37β2 in deoxyhemoglobin.

The $\langle R_{free}^{local-5} \rangle$ profile in Figure 4c also includes three small peaks labeled 1α, 2α, and 3α. Feature 1α corresponds to very small movements in residues 38α−42α which pack against residues responsible for the much larger shifts in feature 4α. These small movements have a significant impact on the $\langle R_{free}^{local-5} \rangle$ statistic because the atoms in residues

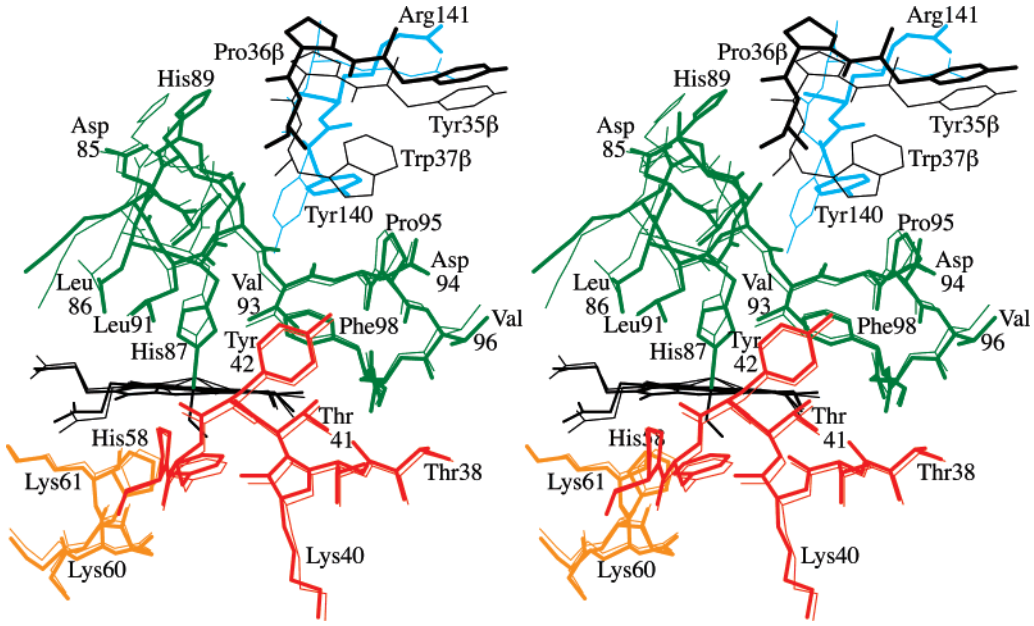

FIGURE 5: Stereodiagram showing the environment of the α1 heme group in wild-type deoxyhemoglobin (thin lines) and βW37A·4O$_2$·0 mM IHP (thick lines) after the α1 subunits were superimposed using the sieve-fit procedure. Color-coding corresponds to the polypeptide segments identified in the $\langle R_{free}^{local-5} \rangle$ profile in Figure 4c. Residues 35β2 through 37β2 are displayed in black lines. For clarity, a water molecule that is bound in the distal heme pocket of deoxyhemoglobin has been omitted from the figure.

38α−42α have very low temperature factors (Figure 4d). Feature 2α corresponds to the distal histidine, His58α, and its flanking residues which shift slightly to accommodate the ligand. Feature 3α corresponds to residues in the EF-corner which shift in response to the large movements of the residues in the adjacent F-helix (feature 4α). There are few small peaks in the rmsd$_5$ and δ_5 profiles that do not cross-validate in the $\langle R_{free}^{local-5} \rangle$ profile. In general, these peaks correspond to regions of the α subunit that have high intrinsic temperature factors and therefore high mobility and large positional variation. These results highlight the ability of the $\langle R_{free}^{local-5} \rangle$ statistic to reveal small structural changes and to distinguish genuine structural perturbations from random fluctuations.

α subunit tertiary structure changes (not shown) very similar to those that occur in βW37A·4O$_2$ are observed for the O$_2$-induced T-to-T$_{High}$ transitions associated with Trp37β cluster mutant hemoglobins and HbA·4O$_2$·10 mM IHP where ρ_{rot} is large. For the O$_2$-induced T-to-T$_{High}$ transitions where ρ_{rot} is small, smaller tertiary structural changes (not shown) are observed in the same regions described above. In all cases, the largest structural change occurs at the end of the F-helix (feature 4α).

Ligand-Induced Changes in the Secondary Structure of the α F-Helix. Detailed analysis of the F-helix hydrogen bonding distances in βV1M, βW37A, βW37A·4O$_2$, and the quaternary R2 structure of carbonmonoxyhemoglobin reveals a ligand-induced secondary structure transition that occurs at the COOH-terminal end of the α F helix. The data shown in Table 5 can be summarized as follows: residues F1 through F5 make only 1→4 hydrogen bonds (the 1→5 distances are greater than 4.0 Å) in all four structures, residue F6 makes only a 1→4 hydrogen bond in the two deoxy structures but it makes bifurcated 1→4/1→5 hydrogen bonds in the βW37A·4O$_2$ and R2 structures (with a weak 1→5 hydrogen bond in βW37A·4O$_2$), residue F7 makes bifurcated 1→4/1→5 hydrogen bonds in the deoxy structures and a weak 1→4 hydrogen bond and a strong 1→5 hydrogen bond in the βW37A·4O$_2$ and R2 structures, and residue F8 (the proximal histidine) makes only a 1→5 hydrogen bond in the deoxy structures but bifurcated 1→5/1→6 hydrogen bonds in the βW37A·4O$_2$ and R2 structures. That is, ligand binding induces a switch in the hydrogen bonding pattern at the COOH-terminal end of the α F-helix. In deoxyhemoglobin, residue F6 has the hydrogen bonding pattern of an α helix, residue F7 has a hydrogen bonding pattern that is midway between an α helix and a π helix, and residue F8 has the hydrogen bonding pattern of a π helix. In both the βW37A·4O$_2$ and R2 structures, residue F6 has a hydrogen bonding pattern that is midway between an α helix and a π helix, residue F7 has a hydrogen bonding pattern that favors a π helix, and residue F8 has the hydrogen bonding pattern of an expanded π helix. Thus ligand binding induces a "bulge" in the COOH-terminal end of the α F-helix of the T$_{High}$ βW37A·4O$_2$ structure that is comparable to the α F-helix bulge in the quaternary R2 structure. Widening the COOH-terminal end of the α F-helix forces Ala88(F9)α into Tyr140α, disrupting the Trp37β cluster (Figure 5).

Ligand-Induced β Subunit Tertiary Structure Changes Associated with T-to-T$_{High}$ Transitions. Figure 6 illustrates the detection and characterization of O$_2$-induced β subunit tertiary structure changes that are associated with the T-to-T$_{High}$ transition in βW37A hemoglobin. The $\langle R_{free}^{local-5} \rangle$ profile in Figure 6c was used to identify and cross-validate six regions of ligand-induced changes in β subunit tertiary structure that are labeled 1β through 6β and highlighted by color-coded bars. The same six regions of tertiary structure change were observed in crystalline wild-type deoxyhemoglobin that was exposed to nitric oxide (*22*). The key structural difference between the response of the β subunits and the response of the α subunits to the binding of ligand (whether the ligand is O$_2$ or NO) is that a ligand-induced movement of the heme group occurs only in the β subunits. The β-heme movement consists of a rotation of approxi-

Table 5: α Subunit F-Helix Hydrogen Bonding Distances[a]

residue (position)	hemoglobin	C=O···HN bond		
		H-donor	type	distance (Å)
Leu80(F1)	βV1M	Ser84(F5)	1→4	2.92
	βW37A	Ser84(F5)	1→4	2.95
	βW37A·4O_2	Ser84(F5)	1→4	2.90
	HbA-R2·4CO	Ser84(F5)	1→4	2.88
Ser81(F2)	βV1M	Asp85(F6)	1→4	2.92
	βW37A	Asp85(F6)	1→4	2.97
	βW37A·4O_2	Asp85(F6)	1→4	3.13
	R2·4CO	Asp85(F6)	1→4	3.02
Ala82(F3)	βV1M	Leu86(F7)	1→4	2.96
	βW37A	Leu86(F7)	1→4	3.04
	βW37A·4O_2	Leu86(F7)	1→4	3.11
	R2·4CO	Leu86(F7)	1→4	3.11
Leu83(F4)	βV1M	His87(F8)	1→4	3.01
	βW37A	His87(F8)	1→4	3.02
	βW37A·4O_2	His87(F8)	1→4	3.08
	R2·4CO	His87(F8)	1→4	2.93
Ser84(F5)	βV1M	Ala88(F9)	1→4	3.15
	βW37A	Ala88(F9)	1→4	3.01
	βW37A·4O_2	Ala88(F9)	1→4	2.90
Asp85(F6)	βV1M	His89(FG1)	1→4	2.99
		Lys90(FG2)	1→5	4.26
	βW37A	His89(FG1)	1→4	2.90
		Lys90(FG2)	1→5	4.25
	βW37A·4O_2	His89(FG1)	1→4	2.80
		Lys90(FG2)	1→5	3.32
	R2·4CO	His89(FG1)	1→4	2.93
		Lys90(FG2)	1→5	3.04
Leu86(F7)	βV1M	Lys90(FG2)	1→4	2.97
		Leu91(FG3)	1→5	2.97
	βW37A	Lys90(FG2)	1→4	2.98
		Leu91(FG3)	1→5	3.02
	βW37A·4O_2	Lys90(FG2)	1→4	3.28
		Leu91(FG3)	1→5	2.84
	R2·4CO	Lys90(FG2)	1→4	3.43
		Leu91(FG3)	1→5	2.73
His87(F8)	βV1M	Leu91(FG3)	1→4	3.75
		Arg92(FG4)	1→5	2.63
		Val93(FG5)	1→6	4.15
	βW37A	Leu91(FG3)	1→4	3.83
		Arg92(FG4)	1→5	2.74
		Val93(FG5)	1→6	4.22
	βW37A·4O_2	Leu91(FG3)	1→4	4.03
		Arg92(FG4)	1→5	2.86
		Val93(FG5)	1→6	3.10
	R2·4CO	Leu91(FG3)	1→4	4.13
		Arg92(FG4)	1→5	3.11
		Val93(FG5)	1→6	3.06

[a] The values in this table are for the α1 subunit. Corresponding values for the α2 subunit are very similar.

mately 5° that shifts pyrrole ring A toward the distal side of the heme pocket and pyrrole ring C by about 0.8 Å toward the NH_2-terminal end of the G-helix on the proximal side of the heme pocket (Figure 7). The ligation-induced movement of the β-heme group in turn induces shifts in residues in regions 2β, 4β, 5β, and 6β (Figure 6) so that optimal packing interactions with the heme are maintained (Figure 7). As in the α subunits, the β distal histidine, His63(E7)β, and flanking residues (region 3β) shift position in order to accommodate the ligand. The residues in region 1β shift because they are in direct van der Waals contact with the residues in region 3β. There are few small peaks in the $rmsd_5$ and δ_5 profiles that do not cross-validate in the $\langle R_{free}^{local-5} \rangle$ profile. In general, these peaks correspond to regions of the β subunit that have high intrinsic temperature factors and therefore high mobility and large positional variation.

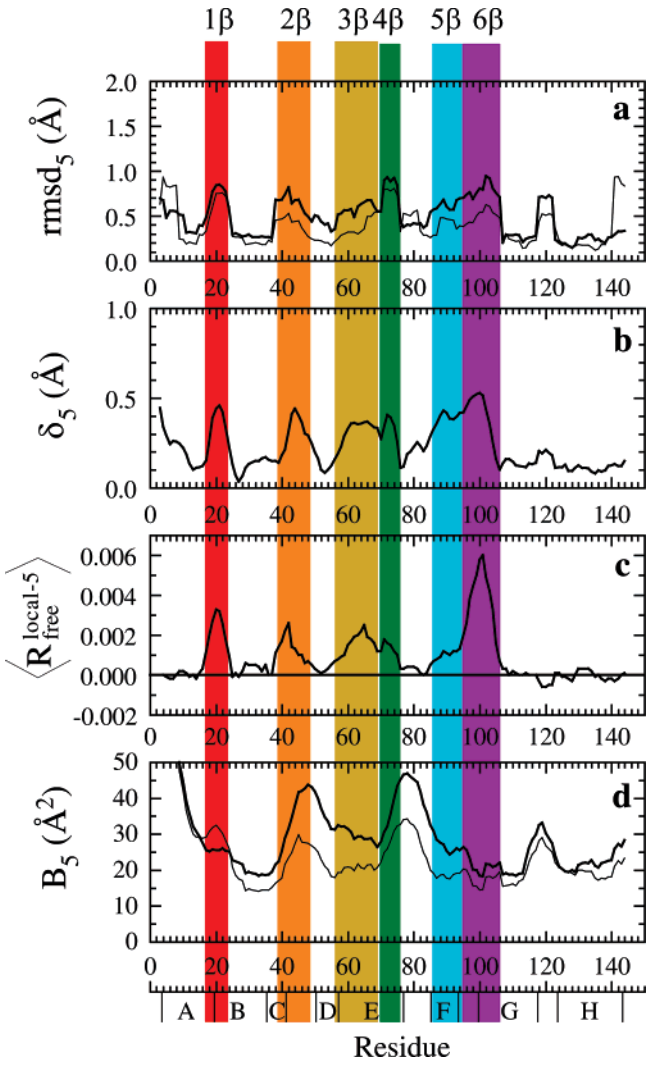

FIGURE 6: Plots of (a) $rmsd_5$, (b) average δ_5, (c) $\langle R_{free}^{local-5} \rangle$, and B_5 for the β subunits (see Figure 4 for parameter definitions).

As in the case of α subunits, β subunit tertiary structure changes very similar to those that occur in βW37A are observed for the O_2-induced T-to-T_{High} transitions associated with Trp37β cluster mutant hemoglobins and HbA·4O_2·10 mM IHP where ρ_{rot} is large (not shown). For the O_2-induced T-to-T_{High} transitions where ρ_{rot} is small, smaller tertiary structural changes are observed in the same regions of the β subunits (not shown).

Heme Relaxation in Liganded Quaternary T_{High} Structures. Ligand-induced changes in the heme Fe out-of-plane distance and the Fe−$N^{\epsilon 2}$His bond length are intrinsic properties of the heme prosthetic group that initiate changes in globin tertiary structure (*7*, *8*, *54*). In particular, crystal structures of oxy and deoxy imidazole−porphyrin model compounds show that the addition of oxygen as an axial ligand results in a ∼0.1 Å shortening of the Fe−imidazole bond and a 0.3−0.4 Å movement of the Fe atom into the porphyrin plane (*54*−*56*). Similar differences are observed in the deoxy quaternary-T and liganded quaternary-R structures of hemoglobin and are the initial events in Perutz's stereochemical mechanism of hemoglobin action (*7*, *8*, *54*).

Small differences in the Fe−$N^{\epsilon 2}$His bond lengths cannot be accurately determine in hemoglobin structures of moderate (3.0 Å to 1.5 Å) resolution. However, estimates of the Fe−

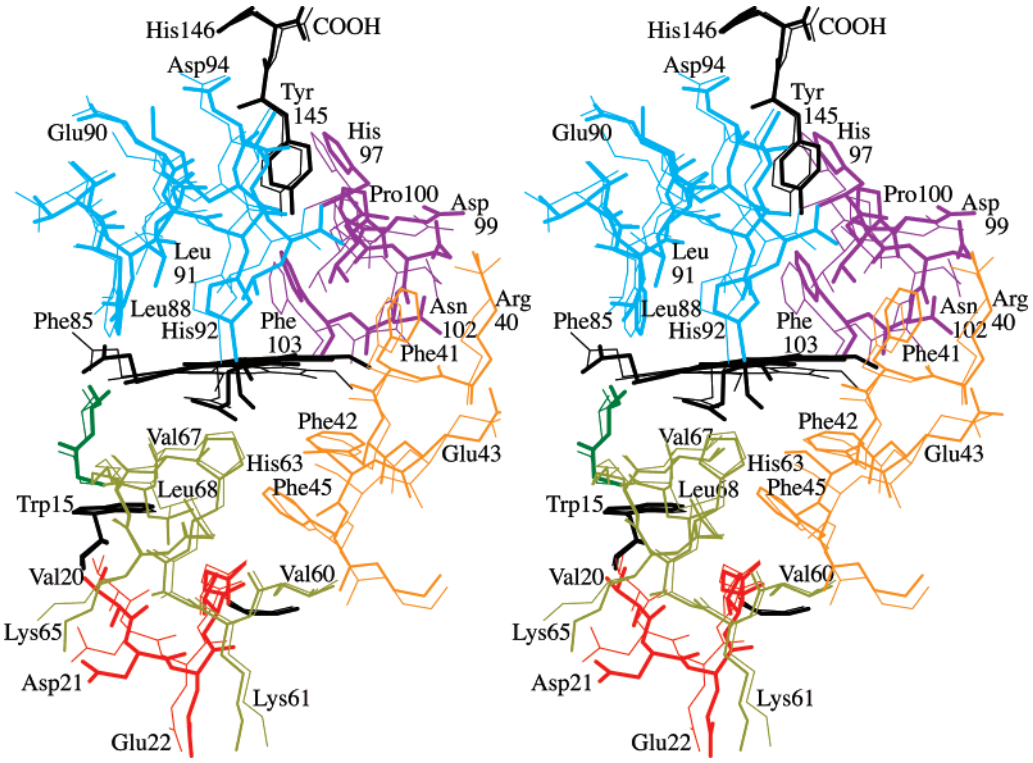

FIGURE 7: Stereodiagram showing the environment of the β1 heme group in wild-type deoxyhemoglobin (thin lines) and βW37A·4O$_2$·0 mM IHP (thick lines) after the β1 subunits were superimposed using the sieve-fit procedure. Color-coding corresponds to the polypeptide segments identified in the $\langle R_{free}^{local-5} \rangle$ profile in Figure 6c.

N$^{\epsilon 2}$His bond lengths can be obtained using a previously described iterative method to minimize restraint bias (*20*). In this method, target values for the Fe−N$^{\epsilon 2}$His bond length are systematically varied until the residual (i.e., the refined value of Fe−N$^{\epsilon 2}$His bond length minus the target value of Fe−N$^{\epsilon 2}$His bond length) is zero. The displacement of the Fe atom from the heme plane can be determined with greater accuracy than the Fe−N$^{\epsilon 2}$His bond length because the heme plane is defined as the least-squares plane of the large 24-atom porphyrin macrocycle and the electron-dense Fe atom can be precisely positioned.

The Fe−N$^{\epsilon 2}$His bond lengths and the heme Fe out-of-plane distances are reported in Table 6 for "zero residual" T$_{High}$ structures refined against diffraction data sets with resolutions between 1.8 Å and 2.9 Å. In deoxyhemoglobin (the deoxy βV1M and deoxy HbA quaternary-T structures in Table 6) the α and β subunit Fe−N$^{\epsilon 2}$His bond lengths are similar with an average value of 2.25 Å, and the Fe atoms of the α and β heme groups are displaced out of the heme plane toward the proximal histidine by −0.60 Å and −0.38 Å, respectively. In the structure of quatermary-R2 carbonmonoxyhemoglobin (which is representative of liganded R^e ensemble structures), the α and β subunit Fe−N$^{\epsilon 2}$His bond lengths have an average value of 2.11 Å, and the Fe atoms of the α and β heme groups are displaced out of the heme plane toward the proximal histidine by only −0.04 Å and −0.07 Å, respectively. In all the T$_{High}$ structures, the α heme Fe atoms have shifted toward the heme planes but remain partially displaced toward the proximal side with average out-of-plane distances of −0.20 ± 0.05 Å. This movement amounts to ∼70% of the total shift between the deoxy quaternary-T and the liganded quaternary-R2 structures. In the β subunits of the T$_{High}$ structures, the Fe atom also appears to shift toward the heme plane with an average out-of-plane distance of −0.24 ± 0.08 Å. However, in this case there is much more variation, especially with the lower resolution data sets.

Table 6: Fe−N$^{\epsilon 2}$His Bond Lengths and Fe Out-of-Plane Distances[a]

hemoglobin	resolution (Å)	ρ_{rot} (deg)	Fe−N$^{\epsilon 2}$His bond length (Å) α	Fe−N$^{\epsilon 2}$His bond length (Å) β	Fe out-of-plane distance[b] (Å) α	Fe out-of-plane distance[b] (Å) β
HbA·4CO (quaternary-R2)	1.7		2.11	2.10	−0.04	−0.07
rHb1.1·Fe^{+3}4CN·0 mM IHP	2.6	8.6	2.09	2.34	−0.14	−0.23
βP36A·4O$_2$·2.2 mM IHP	2.8	5.9	2.07	2.10	−0.23	−0.24
βW37E·4O$_2$·0 mM IHP	2.1	5.6	2.04	2.04	−0.12	−0.17
βW37A·4O$_2$·0 mM IHP	2.2	5.1	2.07	2.04	−0.14	−0.19
αR92A·4O$_2$·2.2 mM IHP	2.9	5.1	2.07	2.08	−0.27	−0.31
βW37Y·4O$_2$·0 mM IHP	2.7	5.0	1.90	1.86	−0.23	−0.31
βW37H·4O$_2$·2.2 mM IHP	2.7	4.8	2.00	1.99	−0.19	−0.27
βW37G·4O$_2$·0 mM IHP	2.1	4.5	2.09	2.04	−0.13	−0.16
HbA·4O$_2$·10.0 mM IHP	2.6	4.3	2.07	2.06	−0.17	−0.38
βW37E(αZn)·2O$_2$·0 mM IHP	2.7	4.0	2.04	1.91	−0.51	−0.32
βV33A·4O$_2$·2.2 mM IHP	2.5	2.3	2.14	2.18	−0.23	−0.12
βH97A·4O$_2$·2.2 mM IHP	2.7	1.4	2.31	1.94	−0.26	−0.37
βP100A·4O$_2$·2.2 mM IHP	2.0	1.3	2.20	2.08	−0.17	−0.15
βY35F·4O$_2$·2.2 mM IHP	1.8	0.9	2.17	2.13	−0.23	−0.17
HbA·4O$_2$·5.0 mM IHP	2.1	0.7	2.32	2.14	−0.22	−0.22
HbA·4O$_2$·2.2 mM IHP	2.2	0.6	2.24	2.05	−0.26	−0.29
deoxy βV1M (quaternary-T)	1.8		2.17	2.26	−0.59	−0.38
deoxy HbA (quaternary-T)	1.9		2.24	2.31	−0.60	−0.37

[a] The bond lengths and Fe out-of-plane distances are the average values for the α or β subunits. [b] The Fe-to-heme plane distance is negative when the Fe atom is on the proximal side of the heme plane. The heme plane is defined as the least-squares plane of the 24-atom porphyrin macrocycle.

The β subunit Fe−N$^{\epsilon 2}$His bond lengths do not appear to correlate with ρ_{rot} and have shortened in all the T$_{High}$ structures with an average value (2.04 ± 0.09 Å) that is close to value observed in quatermary-R2 carbonmonoxyhemo-

globin. In contrast, the α subunit Fe−$N^{\epsilon 2}$His bond lengths appear to be a function of ρ_{rot}. In the T_{High} structures characterized by large interdimer rotations (ρ_{rot} values greater than 4°) the α subunit Fe−$N^{\epsilon 2}$His bond lengths shorten to an average value (2.04 ± 0.06 Å) that is close to value observed in quatermary-R2 carbonmonoxyhemoglobin. However, in the T_{High} structures with ρ_{rot} values less than 4°, the α subunit Fe−$N^{\epsilon 2}$His bond lengths do not shorten; i.e., they have an average value of 2.23 ± 0.07 Å that is very close to that of quaternary-T deoxyhemoglobin. Therefore, it appears that α and β Fe−$N^{\epsilon 2}$His bonds respond differently to the binding of ligand to quaternary-T hemoglobin. In the α subunits, the Fe−$N^{\epsilon 2}$His bond does not shorten in response to ligand binding until the majority of quaternary constraints associated with the Trp37β cluster and the α COOH-termini are broken (see below).

DISCUSSION

The Quaternary Structures of Liganded Hemoglobin Are Distributed Over Two Distinct Ensembles. For many years, the X-ray crystallographic studies on hemoglobin were consistent with the conventional view (i.e., the textbook scenario) that allosteric proteins follow the two-state model of Monod, Wyman, and Changeux (the MWC theory) (*57*). These early X-ray studies demonstrated that the horse hemoglobin tetramer undergoes a large change in quaternary structure upon binding oxygen (*7*). Subsequent X-ray studies at higher resolution seemed to confirm these early results since they showed that both human and horse hemoglobin can adopt the same two stable quaternary structures, one associated with deoxyhemoglobin (the quaternary-T structure) and the other associated with liganded hemoglobin (the quaternary-R structure) (*46*, *58*, *59*). However, in 1991 Smith et al. (*60*) reported that a liganded mutant hemoglobin, carbonmonoxyhemoglobin Ypsilanti, adopts a quaternary structure (the quaternary-Y structure) that is different from the quaternary-R structure of liganded wild-type hemoglobin. The following year Silva et al. (*61*) found that wild-type carbonmonoxyhemoglobin can adopt a "non-R" quaternary structure and that this quaternary structure, the quaternary-R2 structure, was very similar to the quaternary-Y structure. Subsequently, Mueser et al. (*47*) showed that fully liganded hemoglobin can be crystallized in a range of quaternary structures, referred to as the R^e ensemble, that is bounded by the quaternary-R and quaternary-R2 structures. Since the same dimer−dimer contacts are observed in all the R^e ensemble structures, Mueser et al. suggested that "a continuum (or a nearly continuous set) of energetically accessible structures exists for fully liganded hemoglobin between the boundaries set by the quaternary-R and quaternary-R2 structures". This conjecture is supported by the elegant NMR studies of Lukin et al. (*62*) that demonstrated that the quaternary structure of liganded hemoglobin in solution is best represented by an ensemble of low-energy conformations with an average structure midway between the R and R2 conformations. Other crystallographic studies of R2-like structures (*63*, *64*) and structures between R and R2 (*65*, *66*) lend further support to the existence of an R^e ensemble.

The studies reported in this paper show that wild-type and mutant hemoglobins also can adopt a range of T-like quaternary structures, the T_{High} structures, when quaternary-T deoxyhemoglobin is expose to ligand in the crystalline state. Additionally, when mutations disrupt major quaternary constraints in the Trp37β cluster, T_{High} structures are crystallized in the deoxy form and therefore must be present in solution. The fact that a T_{High} structure has been crystallized from solution in the case of the cross-linked cyanomethemoglobin rHb1.1 demonstrates that fully liganded T_{High} structures also exist in solution. We refer to the collection of T_{High} structures as the T^e ensemble.

The transitions between quaternary-T deoxyhemoglobin and the T_{High} quaternary structures have two components, an interdimer rotation of the α1β1 dimer relative to the α2β2 dimer and a correlated intradimer bending motion of the α1 (or α2) subunit relative to the β1 (or β2) subunit. The magnitude of the intradimer bending motion associated with the T-to-T_{High} transitions varies between 0.5° and 3.9° and occurs about an axis that passes through the α1β1 interface. A very similar ∼4° intradimer bending motion, about the same rotation axis, is associated with the T-to-R^e transitions. The interdimer rotation component of the T-to-T_{High} transitions is characterized by a set of screw-rotation axes, the T-to-T^e screw-rotation axes, that are distributed over a narrow range. As shown in Figure 8, the range of T-to-T_{High} screw-rotation axes is very different from the range of screw-rotation axes that define the transitions between quaternary-T deoxyhemoglobin and the liganded structures of the R^e ensemble. The T-to-R^e screw-rotation axes pass through the "hinge region" of the α1β2 interface whereas the T-to-T^e screw-rotation axes pass through the "switch region" of the α1β2 interface. The α direction angles of the T-to-R^e screw-rotation axes are distributed over a range of ∼33° that is bounded by the T-to-R and the T-to-R2 screw-rotation axes, whereas the α direction angles of the T-to-T^e screw-rotation axes are distributed over a range of ∼20° that is bounded by the T-to-βW37A and the T-to-βH97A·IHP·$4O_2$ screw-rotation axes.

Progressive Loss of Dimer−Dimer Contacts in the T^e Ensemble. Since all the structures of the R^e ensemble are characterized by the same small set of dimer−dimer interface contacts, they are energetically similar and should be populated to more or less the same degree in solution (*47*). In contrast, the quaternary-T dimer−dimer contacts are progressively disrupted within the T^e ensemble of structures as the magnitude of the screw-rotation angle ρ_{rot} increases. This important feature of the T^e ensemble is illustrated schematically in Figure 9 where the residues in contact across the dimer−dimer interface of wild-type deoxyhemoglobin and five representative T^e structures are depicted. In this figure, the α1β2, α2β1, and α1α2 contacts are classified as polar interactions, typical nonpolar contacts, and general weak contacts (long contacts between 3.5 Å and 3.8 Å). For clarity, only one line is drawn between each pair of interacting residues and the water bridges are not shown. However, the total number of α1β2, α2β1, and α1α2 contacts, including water bridges, is tallied in Table 7.

The deoxyhemoglobin dimer−dimer interface has a total of 23 polar interactions, 26 typical nonpolar contacts, 81 weak contacts, and 19 water bridges. As indicated in Figure 9a, these stabilizing interactions are distributed more or less uniformly across the length of the dimer−dimer interface. In the HbA·$4O_2$·2.2 mM IHP structure, where ligation causes only a small (0.6°) rotation of the α1β2 and α2β1 dimers relative to each other, dimer−dimer contacts are beginning

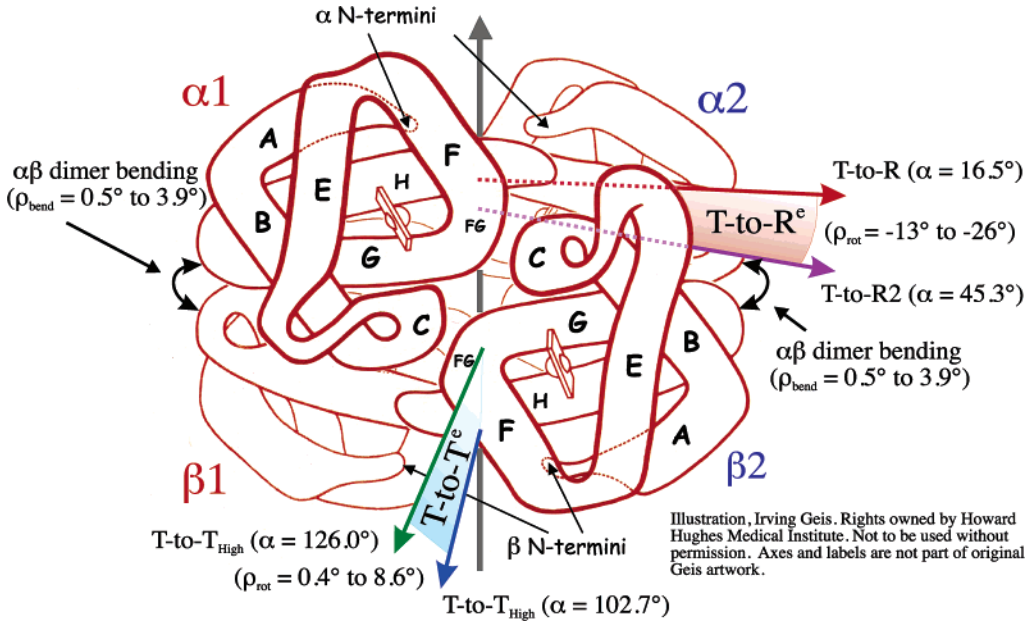

FIGURE 8: The rigid-body screw-rotation axes associated with the T-to-R^e and T-to-T^e transitions superimposed on the Irving Geis drawing of the $\alpha_2\beta_2$ hemoglobin tetramer. [The hemoglobin tetramer is adapted from Figures 1.15 and 2.17 of Dickerson, R. E., and Geis, I. (1983) *Hemoglobin: Structure, Function, Evolution, and Pathology*, The Benjamin/Cummings Co., Inc., Menlo Park, CA.] The molecular dyad is the *y*-axis of the coordinate system and is drawn as a gray arrow through the center of the tetramer. The origin of the coordinate system is at the center of the hemoglobin tetramer, and the *x*-axis is in the plane of the page. The R^e ensemble of transitions is bounded by the screw-rotation axes for the T-to-R (red arrow) and the T-to-R2 (purple arrow) transitions. The T-to-R screw-rotation axis is perpendicular to the dyad axis, has a *y*-intercept of 13.1 Å, and has an α direction angle of 16.5° (i.e., the screw-rotation axis makes an angle of 16.5° with the *x*-axis placing it slightly out of the plane of the page). The T-to-R2 screw-rotation axis is perpendicular to the dyad axis, has a *y*-intercept of 9.2 Å, and has an α direction angle of 45.3°. The T^e ensemble of transitions is bounded by the screw-rotation axes for the T-to-βH97A·4O$_2$·2.2 mM IHP (green arrow) and the T-to-βW37A (blue arrow) transitions. The T-to-βH97A·4O$_2$·2.2 mM IHP screw-rotation axis is perpendicular to the dyad axis, has a *y*-intercept of −6.7 Å, and has an α direction angle of 126.0°. The T-to-βW37A screw-rotation axis is perpendicular to the dyad axis, has a *y*-intercept of −17.7 Å, and has an α direction angle of 102.7°. The T-to-T^e screw-rotation axes are approximately perpendicular to the plane of the page. The intradimer bending component of the T-to-T^e and T-to-R^e transitions is indicated by the double arrow and varies between 0.5° and 3.9°. Note: Illustration, Irving Geis. Rights owned by Howard Hughes Medical Institute. Not to be used without permission. Axes and labels are not part of original artwork.

to be eliminated. Specifically, the small T-to-T$_{High}$ transition between deoxyhemoglobin and HbA·4O$_2$·2.2 mM IHP results in the loss of 4 polar contacts, 16 weak contacts, and one water bridge (Figure 9b and Table 7). Most of the contacts that are lost or weakened are located in the Trp37β1 and Trp37β2 clusters that are highlighted in pink and blue, respectively, in Figure 9. For example, the polar interaction between Asp94α2 and Trp37β1 in the Trp37β1 cluster of deoxyhemoglobin lengthens in the HbA·4O$_2$·2.2 mM IHP structure and is classified as a nonpolar interaction.

A much more dramatic loss of dimer−dimer contacts occurs as the screw-rotation angle, ρ_{rot}, increases to 2.3° in the βV33A·4O$_2$·2.2 mM IHP structure. In this case, the larger T-to-T$_{High}$ transition eliminates a total of 13 polar contacts, 6 nonpolar contacts, 28 weak contacts, and 9 water bridges. Most of the loss in dimer−dimer contacts occurs in the Trp37β1 and Trp37β2 clusters as well as in the region of salt bridges and polar contacts associated with Arg141α1 and Arg141α2 (highlighted in yellow in Figure 9). In contrast, the interactions stabilizing the switch region of the α1β2 and α2β1 interfaces are relatively unperturbed.

In the structures where ρ_{rot} is large (those in Figure 9d, Figure 9e, and Figure 9f where ρ_{rot} varies from 4.3° to 8.6°), no subunit−subunit interactions (not even general weak contacts) remain associated with the Trp37β1 and Trp37β2 clusters or the α COOH-termini (Arg141α1 and Arr141α2). In contrast, even after a dimer−dimer rotation of 8.6° (i.e., the T-to-T$_{High}$ rotation associated with the rHb1.1·Fe^{+3}4CN·0 mM IHP structure), the polar interactions and water bridges stabilizing the switch regions of the α1β2 and α2β1 interfaces remain intact. The stereochemical basis for this difference is that the T-to-T$_{High}$ screw-rotation axes pass through the switch regions (Figure 8). Consequently, even large T-to-T$_{High}$ transitions fail to disrupt key features in the switch region that are diagnostic of the quaternary-T structure. That is, the salt bridge between Lys40α1 and His146β2 and the hydrogen bonds that Tyr42α1 and Asn97α1 make with Asp99β2 (and the symmetry related interactions at the α2β1 interface) are not disrupted, and the side chains of His97β1 and His97β2 remain positioned between the Thr41α2 and Pro44α2 side chains and the Thr41α1 and Pro44α1 side chains, respectively.

It is interesting to note that in the liganded T$_{High}$ structures the Fe−N$^{\epsilon 2}$His(F8) bond lengths in the α subunits do not shorten in response to oxygen binding until ρ_{rot} exceeds 2.3° (Table 6). This coincides with the disruption of all the dimer−dimer interactions associated with the Trp37β1 and Trp37β2 clusters and the α COOH-termini.

Ligand-Induced Tertiary Structure Changes Are Subunit-Specific. A detailed analysis of the ligand-induced tertiary structure changes associated with βW37A has been presented in the Results section. Very similar ligand-induced tertiary structure changes occur in other liganded T$_{High}$ structures where ρ_{rot} is large, and smaller changes occur in the same

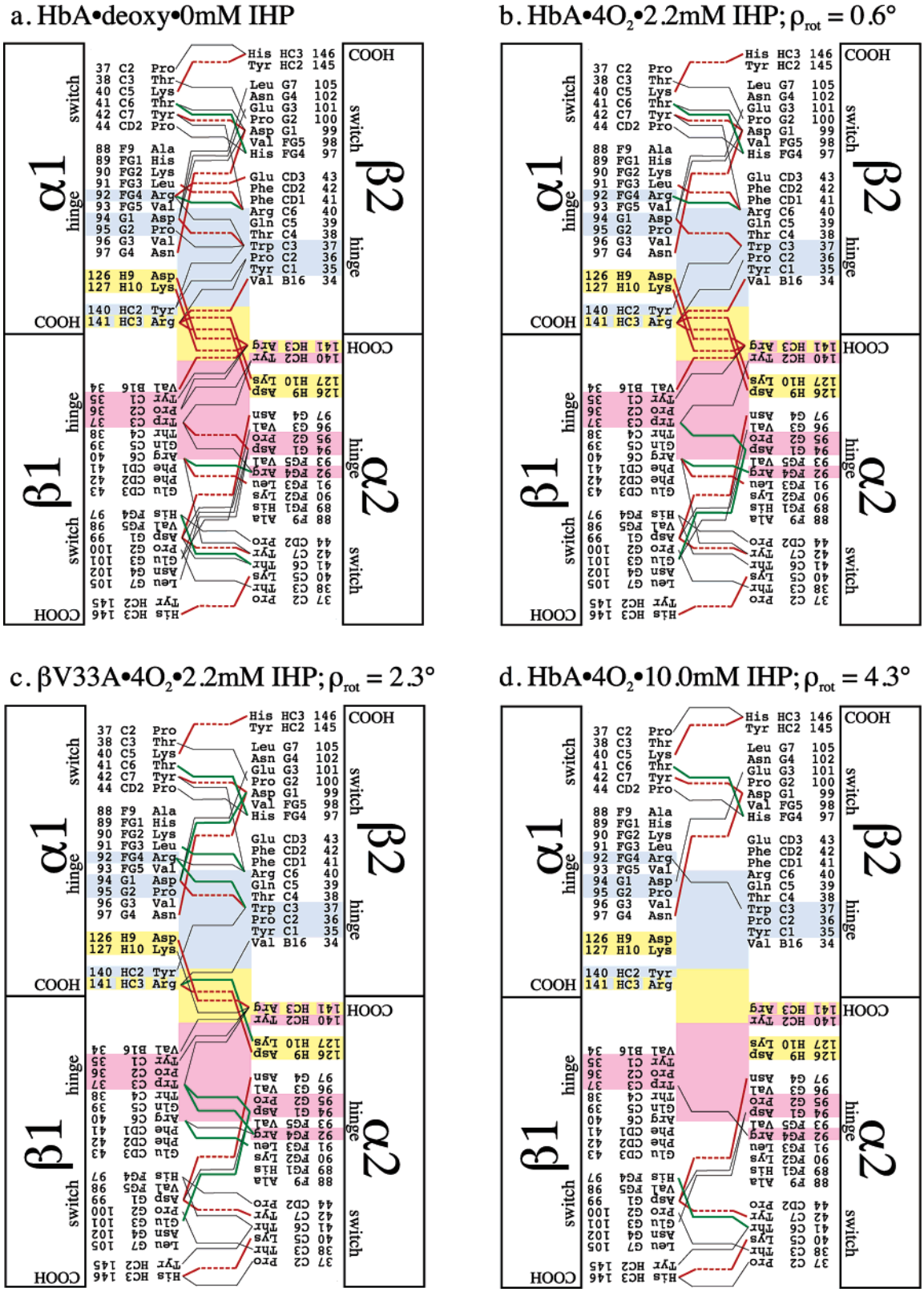

FIGURE 9 (Continued)

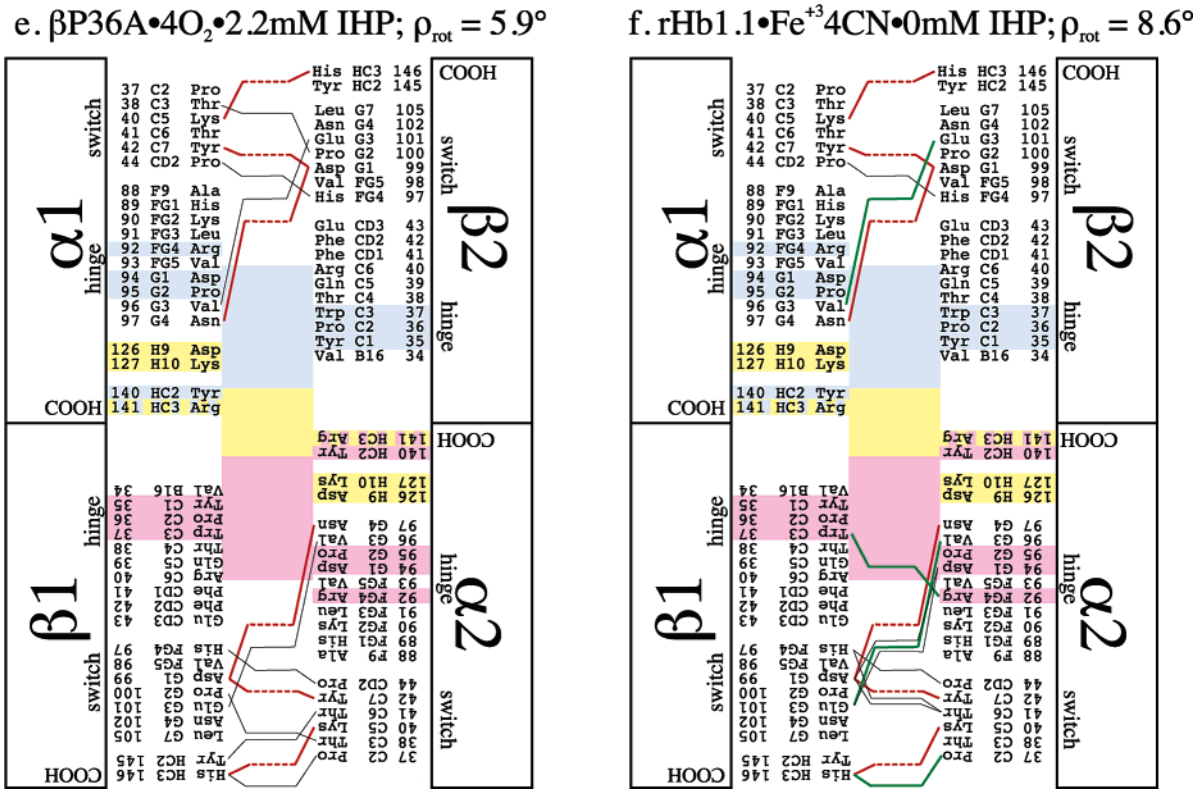

FIGURE 9: Diagrams depicting the residues in contact across the dimer−dimer interface for HbA·deoxy·0 mM IHP (a), HbA·4O_2·2.2 mM IHP (b), βV33A·4O_2·2.2 mM IHP (c), HbA·4O_2·10 mM IHP (d), βP36A·4O_2·2.2 mM IHP (e), and rHb1.1·Fe^{+3}4CN·0 mM IHP (f). The complete dimer−dimer interface consists of $\alpha1\beta2$ contacts (top half of each panel), the dyad-related $\alpha2\beta1$ contacts (lower half of each panel), and the $\alpha1\alpha2$ contacts (center portion of each panel). There are no $\beta1\beta2$ contacts in any of these tetramers. Nonbonded interactions at the dimer−dimer interface are defined as follows; hydrogen bonds (red dashed lines) are defined as interactions of 3.2 Å or less between polar atoms, typical nonpolar interactions (thick green lines) are defined as interactions of 3.5 Å or less between nonpolar atoms or interactions 3.2 Å to 3.5 Å in length between polar atoms, and weak contacts (thin black lines) are defined as any interactions between 3.5 Å and 3.8 Å. The $\alpha2\beta1$ contacts contributing to the Trp37$\beta1$ cluster and the $\alpha1\beta2$ contributing to the Trp37$\beta2$ cluster are highlighted in pink and blue, respectively. The $\alpha1\alpha2$ dimer−dimer interactions are highlighted in yellow. For clarity, only one line is drawn between each pair of interacting residues and the water bridges are not shown. However, the total number of $\alpha1\beta2$, $\alpha2\beta1$, and $\alpha1\alpha2$ contacts, including water bridges, is tallied in Table 7.

Table 7: Interactions Across the $\alpha1\beta2/\alpha2\beta1/\alpha1\alpha2$ Interfaces[a]

hemoglobin	ρ_{rot}	polar contacts	typical nonpolar contacts	weak contacts	water bridges
HbA·deoxy·0 mM IHP		9/8/6 (23)	11/10/5 (26)	31/37/13 (81)	10/9/0 (19)
HbA·4O_2·2.2 mM IHP	0.6	7/6/6 (19)	8/10/8 (26)	27/25/13 (65)	9/9/0 (18)
βV33A·4O_2·2.2 mM IHP	2.3	4/3/3 (10)	8/8/4 (20)	19/26/8 (53)	5/5/0 (10)
HbA·4O_2·10.0 mM IHP	4.3	3/3/0 (6)	6/7/0 (13)	15/17/0 (42)	5/9/0 (14)
βP36A·4O_2·2.2 mM IHP	5.9	3/3/0 (6)	5/2/0 (7)	4/9/0 (13)	1/0/0 (1)
rHb1.1·Fe^{+3}4CN·0 mM IHP	8.6	3/3/0 (6)	7/7/0 (14)	10/14/0 (24)	3/3/0 (6)

[a] ρ_{rot} is the magnitude of the interdimer screw-rotation angle relative to native wild-type deoxyhemoglobin (deoxy HbA). For columns 3 through 6, the number of noncovalent interactions is listed according to the subunit−subunit interfaces $\alpha1\beta2/\alpha2\beta1/\alpha1\alpha2$ followed by the total number of dimer−dimer contacts in parentheses. Polar contacts are defined as atomic interactions of less than 3.2 Å between a pair of polar atoms; typical nonpolar contacts are defined as atomic interactions of less than 3.5 Å between two nonpolar atoms or between a polar and a nonpolar atom; interactions of 3.2−3.5 Å between two polar atoms are counted as nonpolar contacts; water bridges are defined as [polar atom- - -water- - -polar atom] interactions where both water hydrogen bonds are less than 3.2 Å. All interactions between 3.5 and 3.8 Å are classified as weak contacts. For each type of interaction, a contact is counted only if each of the interacting atoms has a temperature factor of 50 $Å^2$ or less.

regions in T_{High} structures where ρ_{rot} is small. In general, within the T^e ensemble, the α and β subunits exhibit very different responses to the binding of ligand.

When ligand binds to the $\alpha1$ subunit, the heme Fe atom shifts toward the heme plane by ~0.40 Å in the T_{High} structures, but the $\alpha1$-heme group does not shift position relative to the α-globin. This movement of the iron pulls the proximal histidine (residue F8) toward the heme plane and forces an α-to-π shift in the hydrogen bonding pattern of the COOH-terminal end of the $\alpha1$ F-helix. The α-to-π transition significantly expands the radius of the end of the $\alpha1$ F-helix, shifting the position of the Ala88$\alpha1$ (residue F9) by ~1.5 Å toward the side chain of Tyr140$\alpha1$. In response, the side chain Tyr140$\alpha1$ is forced into the space occupied by Trp37$\beta2$ disrupting critical quaternary constraints at the dimer−dimer interface. Thus the movement of the $\alpha1$-heme Fe atom initiates an energy transduction pathway in which a small movement of the $\alpha1$ Fe atom is leveraged into a much larger movement that is capable of disrupting quaternary constraints in the Trp37$\beta2$ cluster. In a similar way ligand binding to the $\alpha2$-heme is linked to the disruption of quaternary constraints in the Trp37$\beta1$ cluster.

In the case of the β subunits, ligand binding results in a smaller ($\sim$0.2 Å) shift of the Fe atom toward the β-heme plane in the T_{High} structures, but the β-heme group shifts position significantly relative to the β-globin and no change in the hydrogen bonding pattern at end of the F-helix takes place. In the absence of a change in the secondary structure of the β F-helix, residue Cys93β (the counterpart to Ala88α) is not forced into the side chain of Tyr145β (the counterpart to Tyr140α) and dimer−dimer contacts involving the β-COOH terminus and the β-FG corner are not disrupted. Instead the movement of the β-heme group initiates β-subunit tertiary structure changes in residues in the CD-corner, the F-helix, the E-helix/EF-corner, and the FG-corner/G-helix that are in contact with the heme group. Since oxygen binding to βW37E(αZn) (where only the β subunits can bind oxygen) induces a large T-to-T_{High} transition (Table 3), this transition must be linked to the binding of oxygen at the β heme groups. The analysis presented in Figure 2 suggests that the intradimer bending component of this transition can disrupt quaternary constraints in the Trp37β cluster. This suggests an energy transduction pathway in which ligand-induced β1-heme movement triggers tertiary changes in the β1 subunit that promote $\alpha1\beta1$ dimer bending that disrupts quaternary constraints in the Trp37β2 cluster. Similarly, ligand binding to the β2 heme is linked to the disruption of quaternary constraints in the Trp37β1 cluster via tertiary structure changes in the β2 subunit and the bending of the $\alpha2\beta2$ dimer.

Ackers et al. (*3*) have reported that the binding of the first ligand to an α or β subunit increases the ligand affinity of the unliganded subunit on the liganded dimer, but does not increase the ligand affinity of either subunit on the unliganded dimer. This positive intradimer cooperativity implies that some of the quaternary constraints disrupted by the binding of ligand to the α1 subunit must be the same as those disrupted by the binding of ligand to the β1 subunit and vice versa. The recent mutagenic screen of Noble et al. (*14*) has identified the major region of quaternary constraint to be a cluster of residues centered at Trp37β. Since the α and β pathways described above link ligand binding to the $\alpha1\beta1$ dimer with the Trp37β2 cluster and ligand binding to the $\alpha2\beta2$ dimer with the Trp37β1 cluster, they suggest the following stereochemical basis for intradimer cooperativity. When the first ligand binds to the α1 subunit, quaternary constraints in the $\alpha1\beta2$ interface are disrupted at the Trp37β2 cluster via the α transduction pathway. Likewise when the first ligand binds to the β1 subunit, quaternary constraints in the $\alpha1\beta2$ interface are disrupted at the Trp37β2 cluster via the β transduction pathway. Therefore, the binding of the first ligand to the α1 subunit (or the β1 subunit) will increase the ligand affinity of the β1 subunit (or the α1 subunit) because quaternary constraints at the Trp37β2 cluster common to both subunits have been disrupted. On the other hand, the binding of the first ligand to the α1 subunit (or the β1 subunit) will not increase the ligand affinity of the α2 or β2 subunits because quaternary constraints at the Trp37β1 have not been disrupted.

ACKNOWLEDGMENT

We thank our PPG colleagues (University at Buffalo), Robert Noble, Hilda Hui, and Laura Kwiatkowski, for purifying and assembling the mutant hemoglobin tetramers. We also thank Jamie Weydert, Benjamin Smith, Jeffrey Steinfeld, Mark Klein, Benjamin Davis, and Jason Stroup for help in preparing the mutant globin genes and for expressing them in *E. coli*. We thank Sandy Geis and the Howard Hughes Medical Institute for permission to use the copyrighted artwork of Irving Geis in Figure 8 and the table of contents graphic.

REFERENCES

1. Perutz, M. F. (1989) Mechanisms of cooperativity and allosteric regulation in proteins, *Q. Rev. Biophys. 22*, 139−237.
2. Mills, F. C., Johnson, M. L., and Ackers, G. K. (1976) Oxygenation-linked subunit interactions in human hemoglobin: experimental studies on the concentration dependence of oxygenation curves, *Biochemistry 15*, 5350−5362.
3. Ackers, G. K., Holt, J. M., Huang, Y., Grinkova, Y., Klinger, A. L., and Denisov, I. (2000) Confirmation of a unique intra-dimer cooperativity in the human hemoglobin $\alpha^1\beta^1$ half-oxygenated intermediate supports the symmetry rule model of allosteric regulation, *Proteins Suppl. 4*, 23−43.
4. Antonini, E., Wyman, J., Zito, R., Rossi-Fanelli, A., and Caputo, A. (1961) Studies on carboxypeptidase digests of human hemoglobin, *J. Biol. Chem. 236*, PC60−PC63.
5. Kilmartin, J. V., and Wootton, J. F. (1970) Inhibition of Bohr effect after removal of C-terminal histidines from haemoglobin β-chains, *Nature 228*, 766−767.
6. Kilmartin, J. V., and Hewitt, J. A. (1972) The effect of removal of C-terminal residues on cooperative interactions in hemoglobin, *Cold Spring Harbor Symp. Quant. Biol. 36*, 311−314.
7. Perutz, M. F. (1970) Stereochemistry of cooperative effects in haemoglobin, *Nature 228*, 726−739.
8. Perutz, M. F., Wilkinson, A. J., Paoli, M., and Dodson, G. G. (1998) The stereochemical mechanism of the cooperative effects in hemoglobin revisited, *Annu. Rev. Biophys. Biomol. Struct. 27*, 1−34.
9. Shibayama, N., Morimoto, H., and Kitagawa, T. (1986) Properties of chemically modified Ni(II)−Fe(II) hybrid hemoglobins. Ni-(II) protoporphyrin IX as a model for a permanent deoxy-heme, *J. Mol. Biol. 192*, 331−336.
10. Kavanaugh, J. S., Chafin, D. R., Arnone, A., Mozzarelli, A., Rivetti, C., Rossi, G. L., Kwiatkowski, L. D., and Noble, R. W. (1995) Structure and oxygen affinity of crystalline desArg141α human hemoglobin A in the T state, *J. Mol. Biol. 248*, 136−150.
11. Bettati, S., Kwiatkowski, L. D., Kavanaugh, J. S., Mozzarelli, A., Arnone, A., Rossi, G. L., and Noble, R. W. (1997) Structure and oxygen affinity of crystalline des-His-146β human hemoglobin in the T state, *J. Biol. Chem. 272*, 33077−33084.
12. Hui, H. L., Kwiatkowski, L. D., Karasik, E., Colby, J. E., and Noble, R. W. (2004) Ligand binding to symmetrical FeZn hybrids of variants of human HbA with modifications in the $\alpha1-\beta2$ interface, *Biochemistry 43*, 7843−7850.
13. Wang, D., and Spiro, T. G. (1998) Structure changes in hemoglobin upon deletion of C-terminal residues, monitored by resonance Raman spectroscopy, *Biochemistry 37*, 9940−9951.
14. Noble, R. W., Hui, H. L., Kwiatkowski, L. D., Paily, P., DeYoung, A., Wierzba, A., Colby, J. E., Bruno, S., and Mozzarelli, A. (2001) Mutational effects at the subunit interfaces of human hemoglobin: Evidence for a unique sensitivity of the T quaternary state to changes in the hinge region of the $\alpha1\beta2$ interface, *Biochemistry 40*, 12357−12368.
15. Noble, R. W., Kwiatkowski, A. V., Hui, H. L., Bruno, S., Bettati, S., and Mozzarelli, A. (2002) Correlation of protein functional properties in the crystal and in solution: The case study of T-state hemoglobin, *Protein Sci. 11*, 1845−1849.
16. Karasik, E., Kwiatkowski, L. D., Hui, H. L., Colby, J. E., and Noble, R. W. (2004) Effects of heterotropic allosteric effectors on the equilibrium and kinetics of the reaction of a single ligand molecule with an α or β subunit of deoxygenated HbA, *Biochemistry 43*, 7851−7856.
17. Mihailescu, M. R., Fronticelli, C., and Russu, I. M. (2001) Allosteric free energy changes at the $\alpha1\beta2$ interface of human hemoglobin probed by proton exchange of Trpβ37, *Proteins 44*, 73−78.

18. Kiger, L., Klinger, A. L., Kwiatkowski, L. D., De Young, A., Doyle, M. L., Holt, J. M., Noble, R. W., and Ackers, G. K. (1998) Thermodynamic studies on the equilibrium properties of a series of recombinant βW37 hemoglobin mutants, *Biochemistry 37*, 4336−4345.
19. Kwiatkowski, L. D., Hui, H. L., Wierzba, A., Noble, R. W., Walder, R. Y., Peterson, E. S., Sligar, S. G., and Sanders, K. E. (1998) Preparation and kinetic characterization of a series of βW37 variants of human hemoglobin A: Evidence for high-affinity T quaternary structures, *Biochemistry 37*, 4325−4335.
20. Kavanaugh, J. S., Weydert, J. A., Rogers, P. H., and Arnone, A. (1998) High-resolution crystal structures of human hemoglobin with mutations at tryptophan 37β: Structural basis for a high-affinity T-state, *Biochemistry 37*, 4358−4373.
21. Peterson, E. S., and Friedman, J. M. (1998) A possible allosteric communication pathway identified through a resonance Raman study of four β37 mutants of human hemoglobin A, *Biochemistry 37*, 4346−4357.
22. Chan, N.-L., Kavanaugh, J. S., Rogers, P. H., and Arnone, A. (2004) Crystallographic analysis of the interaction of nitric oxide quaternary-T human hemoglobin, *Biochemistry 43*, 118−132.
23. Hui, H. L., Kavanaugh, J. S., Doyle, M. L., Wierzba, A., Rogers, P. H., Arnone, A., Holt, J. M., Ackers, G. K., and Noble, R. W. (1999) Structural and functional properties of human hemoglobins reassembled after synthesis in *Escherichia coli*, *Biochemistry 38*, 1040−1049.
24. Hernan, R. A., Hui, H. L., Andracki, M. E., Noble, R. W., Sligar, S. G., Walder, J. A., and Walder, R. Y. (1992) Human hemoglobin expression in *Escherichia coli*: Importance of optimal codon usage, *Biochemistry 31*, 8619−8628.
25. Doyle, M. L., Lew, G., De Young, A., Kwiatkowski, L., Wierzba, A., Noble, R. W., and Ackers, G. K. (1992) Functional properties of human hemoglobins synthesized from recombinant mutant β-globins, *Biochemistry 31*, 8629−8639.
26. Kavanaugh, J. S., Rogers, P. H., and Arnone, A. (1992) High-resolution X-ray study of deoxy recombinant human hemoglobins synthesized from β-globins having mutated amino termini, *Biochemistry 31*, 8640−8647.
27. Ward, K. B., Wishner, B. C., Lattman, E. E., and Love, W. E. (1975) Structure of deoxyhemoglobin A crystals grown from polyethylene glycol solutions, *J. Mol. Biol. 98*, 161−177.
28. Metzler, C. M., Rogers, P. H., Arnone, A., Martin, D. S., and Metzler, D. E. (1979) Investigation of crystalline enzyme-substrate complexes of pyridoxal phosphate-dependent enzymes, *Methods Enzymol. 62*, 551−558.
29. Paoli, M., Liddington, R., Tame, J., Wilkinson, A., and Dodson, G. (1996) Crystal structure of T state haemoglobin with oxygen bound at all four haems, *J. Mol. Biol. 256*, 775−792.
30. Wyckoff, H. W., Doscher, M., Tsernoglou, D., Inagami, T., Johnson, L. N., Hardman, K. D., Allewell, N. M., Kelly, D. M., and Richards, F. M. (1967) Design of a diffractometer and flow-cell system for x-ray analysis of crystalline proteins with applications to the crystal chemistry of ribonuclease-S., *J. Mol. Biol. 27*, 563−578.
31. Howard, A. J., Nielsen, C., and Xuong, N. H. (1985) Software for a diffractometer with multiwire area detector, *Methods Enzymol. 114*, 452−472.
32. Leslie, A. G. W. (1992) Recent changes to the MOSFILM package for processing film and image plate data, *Joint CCP4 and ESF-EACBM Newsletter on Protein Crystallography 26*.
33. Evans, P. R. (1997) *Joint CCP4 and ESF-EACBM Newsletter on Protein Crystallography 33*, 22−24.
34. Collaborative Computational Project. (1994) *Acta Crystallogr. D50*, 760−763.
35. Kavanaugh, J. S., Rogers, P. H., Case, D. A., and Arnone, A. (1992) High-resolution x-ray study of deoxyhemoglobin Rothschild 37βTrp→Arg: a mutation that creates an intersubunit chloride-binding site, *Biochemistry 31*, 4111−4121.
36. Brünger, A. T. (1992) *X-PLOR*, version 3.1, Yale University Press, New Haven.
37. Hendrickson, W. A. (1985) Stereochemically restrained refinement of macromolecular structures, *Methods Enzymol. 115*, 252−270.
38. Murshudov, G., Vagin, A. A., and Dodson, E. J. (1997) Refinement of molecular structures by the maximum-likelihood method, *Acta Crystallogr. D53*, 240−255.
39. Jones, T. A. (1985) Diffraction methods for biological macromolecules. Interactive computer graphics: FRODO, *Methods Enzymol. 115*, 157−171.
40. Cambillau, C. (1989) *Silicon Graphics Geometry Partners Directory*, p 61, Silicon Graphics, Mountain View, CA.
41. Brünger, A. T. (1992) Free R-value—A novel statistical quantity for assessing the accuracy of crystal-structures, *Nature 355*, 472−474.
42. Brünger, A. T. (1993) Assesment of phase accuracy by cross validation: the free R value—Methods and Applications, *Acta Crystallogr. D49*, 24−36.
43. Waller, D. A., and Liddington, R. C. (1990) Refinement of a partially oxygenated T state human haemoglobin at 1.5 Å resolution, *Acta Crystallogr. B 46*, 409−418.
44. Arnone, A., and Perutz, M. F. (1974) Structure of inositol hexaphosphate—human deoxyhaemoglobin complex, *Nature 249*, 34−36.
45. Cox, J. M. (1967) Mathematical methods used in the comparison of the quaternary structures, *J. Mol. Biol. 28*, 151−156.
46. Baldwin, J., and Chothia, C. (1979) Haemoglobin: The structural changes related to ligand binding and its allosteric mechanism, *J. Mol. Biol. 129*, 175−220.
47. Mueser, T. C., Rogers, P. H., and Arnone, A. (2000) Interface sliding as illustrated by the multiple quaternary structures of liganded hemoglobin, *Biochemistry 39*, 15353−15364.
48. Gerstein, M., and Chothia, C. (1991) Analysis of protein loop closure: Two types of hinges produce one motion in lactate dehydrogenase, *J. Mol. Biol. 220*, 133−149.
49. Kavanaugh, J. S., Weydert, J. A., Rogers, P. H., Arnone, A., Hui, H. L., Wierzba, A. M., Kwiatkowski, L. D., Paily, P., Noble, R. W., Bruno, S., and Mozzarelli, A. (2001) Site-directed mutations of human hemoglobin at residue 35β: A residue at the intersection of the $\alpha1\beta1$, $\alpha1\beta2$, and $\alpha1\alpha2$ interfaces, *Protein Sci. 10*, 1847−1855.
50. Kroeger, K. S., and Kundrot, C. E. (1997) Structures of a hemoglobin-based blood substitute: Insights into the function of allosteric proteins, *Structure 5*, 227−237.
51. Perutz, M. F., Muirhead, H., Cox, J. M., and Goaman, L. C. (1968) Three-dimensional Fourier synthesis of horse oxyhaemoglobin at 2.8 A resolution: the atomic model, *Nature 219*, 131−139.
52. Nichols, W. L., Zimm, B. H., and Ten Eyck, L. F. (1997) Conformation-invariant structures of the $\alpha1\beta1$ human hemoglobin dimer, *J. Mol. Biol. 270*, 598−615.
53. Kavanaugh, J. S., Rogers, P. H., Arnone, A., Hui, H. L., Wierzba, A., DeYoung, A., Kwiatkowski, L. D., Noble, R. W., Juszczak, L. J., Peterson, E. S., and Friedman, J. M. (2005) Intersubunit interactions associated with Tyr42α stabilize the Quaternary-T tetramer but are not major quaternary constraints in deoxyhemoglobin, *Biochemistry 44*, 3806−3820.
54. Perutz, M. F. (1979) Regulation of oxygen affinity of hemoglobin: Influence of structure of the globin on the heme iron, *Annu. Rev. Biochem. 48*, 327−386.
55. Jameson, G. B., Molinaro, F. S., Ibers, J. A., Collman, J. P., Brauman, J. I., Rose, E., and Suslick, K. S. (1978) Structural changes upon oxygenation of an iron(II)(porphyrinato)(imidazole) complex, *J. Am. Chem. Soc. 100*, 6769−6770.
56. Jameson, G. B., Rodley, G. A., Robinson, W. T., Gagne, R. R., Reed, C. A., and Collman, J. P. (1978) Structure of a dioxygen adduct of (1-methylimidazole)-*meso*-tetrakis($\alpha,\alpha,\alpha,\alpha$-*o*-pivalamidophenyl)porphinatoiron(II). An iron dioxygen model for the heme component of oxymyoglobin, *Inorg. Chem. 17*, 850−857.
57. Monod, J., Wyman, J., and Changeux, J.-P. (1965) On the nature of allosteric transitions: a plausible model, *J. Mol. Biol. 12*, 88−118.
58. Shaanan, B. (1983) Structure of human oxyhaemoglobin at 2.1 Å resolution, *J. Mol. Biol. 171*, 31−59.
59. Fermi, G., Perutz, M. F., Shaanan, B., and Fourme, R. (1984) The crystal structure of human deoxyhaemoglobin at 1.74 Å resolution, *J. Mol. Biol. 175*, 159−174.
60. Smith, F. R., Lattman, E. E., and Carter, C. W. J. (1991) The mutation β99Asp→Tyr stabilizes Y—a new, composite quaternary state of human hemoglobin, *Proteins 10*, 81−91.
61. Silva, M. M., Rogers, P. H., and Arnone, A. (1992) A third quaternary structure of human hemoglobin A at 1.7-Å resolution, *J. Biol. Chem. 267*, 17248−17256.
62. Lukin, J. A., Kontaxis, G., Simplaceanu, V., Yuan, Y., Bax, A., and Ho, C. (2003) Quaternary structure of hemoglobin in solution, *Proc. Natl. Acad. Sci. U.S.A. 100*, 517−520.
63. Smith, F. R., and Simmons, K. C. (1994) Cyanomet human hemoglobin crystallized under physiological conditions exhibits the Y quaternary structure, *Proteins 18*, 295−300.

64. Sutherland-Smith, A. J., Baker, H. M., Hofmann, O. M., Brittain, T., and Baker, E. N. (1998) Crystal structure of a human embryonic haemoglobin: The carbonmonoxy form of gower II ($\alpha_2\epsilon_2$) haemoglobin at 2.9 Å resolution, *J. Mol. Biol. 280*, 475−484.
65. Safo, M. K., and Abraham, D. J. (2001) The X-ray structure determination of bovine carbonmonoxy hemoglobin at 2.1 Å resoultion and its relationship to the quaternary structures of other hemoglobin crystal forms, *Protein Sci. 10*, 1091−1099.
66. Biswal, B. K., and Vijayan, M. (2001) Structure of human methaemoglobin: The variation of a theme, *Curr. Sci. 81*, 1100−1105.

BI047813A